NASA Contractor Report 4352

Description and Evaluation of an Interference Assessment Method for a Slotted-Wall Wind Tunnel

William B. Kemp, Jr.

CONTRACT NAS1-18585
APRIL 1991

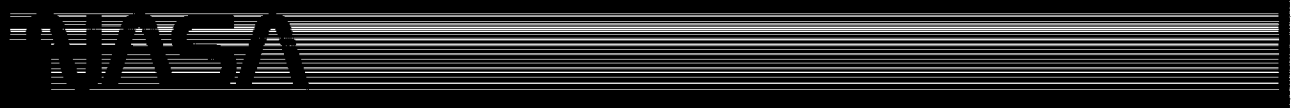

NASA Contractor Report 4352

Description and Evaluation of an Interference Assessment Method for a Slotted-Wall Wind Tunnel

William B. Kemp, Jr.
ViGYAN, Inc.
Hampton, Virginia

Prepared for
Langley Research Center
under Contract NAS1-18585

National Aeronautics and
Space Administration
Office of Management
Scientific and Technical
Information Division

1991

Summary

A wind-tunnel interference assessment method applicable to test sections with discrete finite-length wall slots is described. The method is based on high order panel method technology and uses mixed boundary conditions to satisfy both the tunnel geometry and wall pressure distributions measured in the slotted-wall region. Both the test model and its sting support system are represented by distributed singularities. The method yields interference corrections to the model test data as well as surveys through the interference field at arbitrary locations. These results include the equivalent of tunnel Mach calibration, longitudinal pressure gradient, tunnel flow angularity, wall interference, and an inviscid form of sting interference. Alternative results which omit the direct contribution of the sting are also produced.

The method has been applied to the National Transonic Facility at NASA Langley Research Center for both tunnel calibration tests and tests of two models of subsonic transport configurations. Accuracy of the results is limited by scatter in the measured wall pressures arising from imperfections in the wall orifice installation. Although the magnitude of wall interference predicted by traditional methods for the two test models was within the assessment accuracy limitation, trends characteristic of the predicted interference were apparent in the assessed interference distributions. Significant levels of support interference were found for one model having an upper swept strut support attached to a displaced sting whereas the sting interference for the other model supported by a sting emerging symmetrically from the blunt model base was limited to modest contributions to blockage and longitudinal buoyancy interference.

Introduction

During the decade of the 1970s the emphasis in transonic wind tunnel testing underwent a shift from exploration of transonic flow phenomena to refinement of aircraft design. Accordingly, major new initiatives were undertaken to enhance the accuracy of the tunnel test results as applied to the aircraft in flight. One such initiative was the resurgence of research effort on the problem of accounting for the presence of the test section walls and their interference with the flow at the test model.

Improved accounting for wall interference was deemed necessary because of the difficulty in expressing accurately the characteristics of the slotted or perforated walls used for transonic tunnels in the form of boundary conditions for the classical wall interference theory, and because of the inability of that theory to account for the inherent nonlinearity of transonic flows. The renewed research in this area was stimulated by the newly developed capability for numerical solution of transonic flow problems, (ref. 1) and by the publication of the adaptive wall concept, conceived and described independently by Ferri and Baronti (ref. 2), and by Sears (ref. 3). Three different research targets emerged. One was improved interference prediction through refined understanding and representation of the flow physics of ventilated walls (see refs. 4, 5 and 6 for slotted walls and ref. 7 for perforated walls). A second target was elimination of wall interference through physical implementation of the adaptive wall concept (an annotated bibliography is given in ref. 8); and a third was improved interference corrections through assessment of the wind tunnel flow as defined by flow properties measured near the tunnel walls. The technology of this third area has become known as wall-interference assessment and correction (WIAC).

For two-dimensional airfoil test facilities, numerous variants of assessment schemes have been proposed and can be categorized, as in reference 9, according to the type and location of measured flow data, representation of the test model, and use of linearizing assumptions in the flow equations and in separating the model and tunnel effects. In the scheme of reference 10, satisfaction of measured pressure distributions is the primary boundary condition used both on the model surface and near the tunnel walls, permitting interference assessment free of linearizing assumptions and without specification of an equivalent inviscid shape of the test airfoil.

For application to three-dimensional tests, the amount of measured flow data required for definition of computational boundaries can become very large. In particular, the use of measured flow data as an inner boundary specification at the test model surface appears highly impractical. A relatively small number of three-dimensional assessment procedures have been developed to the point of extensive evaluation. In the procedures of references 11 and 12, which solve a linearized governing equation, an inner boundary is avoided by representing the test model as a set of singularities with locations and strengths defined a priori to be consistent with the model geometry and measured forces. In the transonic procedure of reference 13 and both of the WIAC procedures described in reference 7, a Neumann condition is imposed at the inner boundary on the model surface; and iterative adjustments are made either to the angle of attack to match the measured lift or to model shape distortion modes to approximate a measured flow angularity distribution at the outer boundary.

In all of the above three-dimensional procedures, pressures measured at an outer boundary on or near the tunnel walls are interpolated to appropriate boundary points and imposed as outer boundary conditions, usually in the form of longitudinal velocity perturbations. When these methods are applied in perforated-wall tunnels, the outer boundary pressures usually are measured on tubes or rails of such dimensions that disturbances from discrete perforations are effectively averaged. In slotted-wall tunnels, however, avoidance of discrete slot effects would require making the pressure measurements at a distance of the order of the slot spacing inward from the slotted walls. Meeting this requirement could introduce awkward instrumentation problems and demand higher near field fidelity in the test model representation than would measuring pressures on the walls between slots, a location subject to significant discrete slot effects.

An interference assessment procedure which was developed specifically for use in slotted-wall wind tunnels is described in the present paper. A key requirement was that it be suitable for use in slotted-wall wind tunnels in which the pressures used as outer boundary conditions on the computed tunnel flow are measured on the test section walls between slots. It follows that the flow perturbations arising from the discreteness of the slots and felt at the pressure orifices must be represented appropriately in the flow computation. Because the slot discreteness perturbations depend on the magnitude and distribution of the flow through the slots, it is important that other tunnel and installation features capable of perturbing the measured pressures (such as wall divergence setting or the model support sting) also be represented in the flow computation so that the slot flux will not be distorted to compensate for the absence of such perturbing features.

The slotted-tunnel simulation method described in reference 14 was developed with the intention of being converted to an interference assessment method using the concepts noted above. The assessment method of the present paper is the result of that conversion; therefore, many of the characterizing features of the simulation method are carried over to the assessment method. These include representation of the outer boundary (the tunnel walls) by a high order panel method, and the use of line sources with piecewise linear strength distributions to represent discrete finite-length slots in a special panel network for slotted walls. The outer boundary of the assessment method uses a mixture of Neumann conditions to specify known shape characteristics and measured pressure constraints to control only those boundary phenomena which cannot be specified accurately a priori. Accordingly, the theoretical slot flux boundary conditions of the reference 14 simulation are replaced by measured pressure constraints in the assessment procedure. A concise description of the method is given in reference 15 with some early examples of its application.

The present paper describes the major features of this assessment procedure, and illustrates its application to the National Transonic Facility (NTF) at NASA Langley Research Center. The NTF test section has solid side walls and slotted top and bottom walls with reentry flaps at the slot terminations. Results illustrating the effects of variations in wall divergence and reentry flap settings are presented as are interference assessment results from tests of two aircraft models.

Symbols

$\mathbf{A}$	square coefficient matrix
a_t	velocity of sound at stagnation conditions, m/sec
$\mathbf{b}$	column vector of knowns
$\mathbf{C}$	banded smoothing matrix
C	cross section area of test section, m^2
C_D	drag coefficient
C_L	lift coefficient
C_M	pitching-moment coefficient
C_p	pressure coefficient
c	chord of local airfoil section, m
$\bar{c}$	reference chord of model, m
c_{l_α}	local section lift curve slope, per rad
e	norm of $\boldsymbol{\epsilon}$

F	reentry source panel strength factor
f	inner index smoothing factor
g	outer index smoothing factor
Δh	step height at end of reentry region, m
i_t	tail incidence setting, deg
M	Mach number
M_R	Mach number of uniform reference flow
q	parameter in reentry region source shape function
R_u	Reynolds number based on length unit of $0.1\sqrt{C}$
S	Reference wing area of model, m
s	source shape function for reentry region panels
u, v, w	perturbation velocity components in x, y, and z directions, respectively, relative to reference flow velocity
X	Dimensionless longitudinal coordinate in reentry region
$\mathbf{x}$	column vector of unknowns
x, y, z	cartesian coordinates, x downstream, y lateral, z upward, m
Δy	spanwise extent of wing area element associated with local spanwise station
α	flow angularity, positive upward, deg
α_S	flow rate through wall slot expressed as equivalent homogeneous wall flow angularity, deg
γ	scalar smoothing multiplier
Δ	prefix for interference increment or interference correction
$\boldsymbol{\epsilon}$	vector of deviations from boundary conditions
Σ	reference strength for a longitudinal row of reentry region source panels
σ	source panel strength, relative to reference flow velocity

Subscripts:

B	bottom wall
b	arising from longitudinal buoyancy
c	on tunnel center line
$c/4$	at local quarter-chord point
$c/2$	at local half-chord point
D	downstream
i, j	array indices
LE	leading edge
ref	at model moment reference point
s	smoothed
sc	arising from streamline curvature
T	top wall

TE	trailing edge
theo	interference predicted by theory
tot	total interference
U	upstream
u	arising from interference upwash
W	wing
wall	interference omitting direct contribution of sting

Superscript:

T	transpose

Description of the Assessment Method

Conceptual Basis

The interference assessment method of the present paper, like those of references 11 and 12, makes use of solutions of the linearized potential equation subject to constraints imposed on an outer boundary located at or near the tunnel walls. It was noted in reference 12 that such solutions remain valid as long as embedded supersonic pockets do not extend to the tunnel walls. Because of the linear governing equation, the tunnel flow can be represented as the superposition of a free air flow over the model and a wind tunnel interference flow. In the methods of references 11 and 12, all boundary conditions are derived from measured pressures which are converted, by subtracting the influence of the test model, to Dirichlet conditions on the longitudinal velocity component of the interference field. The longitudinal interference velocity component at the model is then obtained directly from the solution and the vertical component is calculated by integrating the irrotationality condition from measured or assumed flow angles far upstream.

The present method differs, however, in that the boundary conditions are of mixed form so that a combination of measured pressures and local tunnel wall slopes can be specified. For convenience, these are formulated as constraints on the total tunnel flow. The test model is represented as a system of singularities of known strength as are other features capable of influencing the flow at the walls such as the model support sting. Inclusion of such features is necessary to assure that the magnitude and distribution of flow through the wall slots and, therefore, the slot discreteness effects felt in the measured pressures, are properly represented. After solving for all unknown singularity strengths, the longitudinal and vertical components of interference velocity are calculated at the model and at other prescribed locations by summing the influences of all singularities except those representing the test model. The "total interference" field so determined includes, of course, the effects of the inviscid sting representation as specified in the assessment problem. An alternative form designated the "wall interference" field is calculated by omitting both the test model and sting singularities from the post-solution influence summation. This alternative form is useful for studies aimed at understanding the behavior of the slotted tunnel walls, and even for tunnel interference corrections to the model data in case sting interference corrections from other sources are available and preferred. The reader should understand that although the direct influence of the sting is omitted from the "wall interference" field, some indirect influence remains because the wall pressures used as boundary conditions were measured with the sting in place and the wall singularities were solved to satisfy all boundary conditions for the total tunnel flow. For both forms of interference, increments in Mach number and flow angle are calculated from the velocity components. The distributions of these interference increments over the test model are processed to determine corrections to the model test data for the effective values of blockage and upwash at the wing and tail, their longitudinal gradients, and the spanwise variation of upwash over the wing.

Some users of tunnel interference assessment methods (for two- or three-dimensional testing) choose to impose as outer boundary conditions the difference between pressure coefficients measured during the model test and those measured with the model removed. The empty tunnel pressures serve as tare data containing anomolies associated with individual orifice characteristics and, to the extent that such anomolies are unchanged by inserting the model, they are removed by subtracting the tare data. The improvement in quality of the wall pressure data can be impressive, particularly for three-dimensional tests where the model signature in the wall pressures is generally very small. Of course, the use of tared pressures also removes the effects of any other tunnel features common to both tests such as wall divergence or a model support system and prevents the assessment results from reporting the

effects of such features. As a result, wall interference corrections obtained from tared pressure assessments must be used in conjunction with the usual Mach calibration and flow angularity corrections whereas those from untared pressure assessment tend to be self-calibrating. This subject is discussed more fully in reference 9. For assessment methods in which the outer boundary specification is derived completely from measured pressures, the use of tared pressures is straightforward as long as the model-in and model-out test conditions are otherwise identical. If tared pressures are used with the present method, however, the assessment problem should be specified with the sting support omitted and the tunnel walls represented as flat parallel walls. The discrete slot modeling is still appropriate so that the discrete slot effects on wall pressure induced by slot flows arising only from the presence of the model will be accounted for.

Formulation of Assessment Method

Panel Method Usage. The method of the present paper is implemented in a computer program which provides the modular building blocks necessary to assemble an aerodynamic panel method problem, express it as a linear matrix equation, solve it for the unknown singularity strengths, and perform a post-solution analysis of the aerodynamic flow represented by the solution. Many of the panel method modules are essentially the same as those used for the slotted-wall tunnel simulation of reference 14 which, in turn, was based on a higher order panel method code written at NASA Langley Research Center for use in the panel method technology study of reference 16. Certain new features were added during the development of the present method and these will be described in subsequent sections of this paper. Although the computer program offers much flexibility, the interference assessment method described herein is implemented as a very specific way of assembling the program's capabilities. The present implementation has been developed specifically for test sections having slotted top and bottom walls and solid side walls.

Figure 1 illustrates the types of panel networks used to form the outer boundary of a typical slotted tunnel assessment problem. Only the paneling on one side of a vertical plane of symmetry is specified in detail, with that on the other side included using symmetry considerations. The tunnel flow domain is a rectangular parallelepiped enclosed with networks of doublet panels except at the upstream face where the doublet panel is omitted to force continuity of the perturbation potential in the tunnel flow with that in the flow outside of the tunnel domain which is constrained to be unperturbed. The doublet networks representing the tunnel top, bottom, and side walls use a biquadratic distribution of doublet strength over the panels with continuity across panel boundaries enforced in a least square sense. In figure 1, each panel network is annotated with (U) or (P) to denote whether the singularity strengths in that network are unknown or prescribed, respectively.

The boundary condition imposed at the center of each doublet panel and at the edges of doublet panel networks constrains the flow outside the tunnel domain to have a perturbation potential of zero (for an equivalent homogeneous representation of slotted walls). This same constraint is imposed at the panel centers of the upstream and downstream faces of the tunnel flow domain. The effect of this constraint on the interior flow is equivalent to a Neumann condition controlled by specifying the strength of source panels superimposed over the bounding doublet panels. Those regions of the boundary shown on figure 1 as having no source panels represent a solid wall with zero slope by requiring the normal component of interior flow velocity to be continuous with that in the unperturbed outer flow. The sidewall source panels shown near the downstream end of the tunnel flow boundary are used to model the bending of the side wall into the divergent diffuser by prescribing source panel strengths equal to the diffuser wall slope. Similarly, on the top wall, a prescribed source strength network having two large panels is included to model the wall slopes in the slotted region and in the diffuser region.

Representation of Slotted Walls. Details of the use of the slotted-wall and reentry region source networks are described with the aid of figure 2 which relates these networks to the slotted wall geometry. The slotted-wall source network is a special network of source panels and lines and is essentially the same as that developed for the simulation of reference 14 to work in conjunction with the biquadratic doublet panels (fig. 1) to represent a discretely slotted tunnel wall. This source network performs a simultaneous combination of two quantitatively identifiable functions. The first is to provide a panel source distribution equivalent to the flux through an equivalent homogeneous representation of the slotted wall, and the second is to concentrate this transversely distributed flux into the discrete line sources at the slot locations. The influence of the latter discretization function on the interior tunnel flow produces the desired manifestation of discrete slot effects but its influence on the outer flow cannot be suppressed simply by constraining the outer flow perturbation potential to zero at the panel centers. Consequently, the influence of just the discretization function is allowed to exist in the outer flow as well as in the inner flow. This is achieved by omitting this influence while evaluating the zero perturbation potential constraint imposed on

the outer flow. The effectiveness of this representation in satisfying solid wall characteristics between slots while retaining the longitudinal wall flux distribution matching that of the equivalent homogeneous wall was demonstrated in reference 14.

The line source strengths at the quantification points indicated by the circle symbols on figure 2 constitute the set of unknowns in the slotted-wall source network. The line source strengths vary linearly between quantification points and are zero by definition at the upstream and downstream borders of the network. The panel source strengths have a bilinear distribution within each panel and are linked to the line source strengths in such a way that the homogeneous wall and flux discretization functions are combined properly. Wall pressure coefficients measured in longitudinal rows (one row per slot) and interpolated longitudinally to the control point locations indicated by the $\times$ symbols on figure 2 constitute the network constraints. The transverse locations of the pressure control point rows relative to the slots should match those of the pressure orifice rows for proper representation of discrete slot effects.

The Pressure Coefficient Boundary Condition. The linearized potential equation which underlies the panel method formulation uses a small perturbation assumption to treat compressibility. Although expressing the wall pressure constraint by the small perturbation form $C_p = -2u$ is mathematically consistent with this assumption, experience with the simulation method showed that in post-solution flow analysis, the large perturbation behavior of this form is less than satisfactory. For example, if the flow approaches a stagnation point where $u = -1$, it is disconcerting to see the pressure coefficient approach a value of 2. For this reason, pressure coefficients were calculated in the simulation method using the exact compressible function of flow velocity. In the assessment method, the same approach is used in post-solution flow analysis, and for consistency, the exact form is used also to express the wall pressure constraints. The exact expression for C_p as a function of the perturbation velocity components may be solved for the linear term in u to yield

$$u = \frac{1}{.4M_R^2}\left[1 - \left(1 + .7M_R^2 C_p\right)^{2/7}\right] - \frac{1}{2}(u^2 + v^2 + w^2) \tag{1}$$

where a value of 1.4 has been used for the ratio of specific heats. In the matrix equation solution, the term involving squares of u, v, and w is set initially to $\frac{1}{2}u^2$ and then is updated iteratively.

As part of the development of the interference assessment method, a study was made to determine the optimal longitudinal locations of the control points at which the pressure boundary condition is imposed. With many of the locations examined, the iterative solution was found to diverge until an artificial smoothing capability (described in a subsequent section of this paper) was introduced to suppress a divergent spacial oscillatory mode. The solution behavior was found to be poorest when the control points were located near the longitudinal position of the line source quantifying points. With the control points located about one half of the line segment length upstream of the quantifying points, only a very small amount of smoothing was needed to stabilize the solution. Stable solutions with no artificial smoothing were found with the control points located longitudinally about one half of the line segment length downstream of the line source quantifying points. This location, shown in figure 2, has been adopted as the standard.

Development of the Reentry Region Model. In many slotted-wall tunnels, the region at the downstream ends of the slots where the transition from slotted test section walls to solid diffuser walls occurs, is characterized by complex geometry and may have adjustable reentry flaps. In this region, a layer combining viscous shear with vortices shed from tapered slot edges serves to transfer energy from the tunnel flow to the low energy flow reentering the tunnel from the plenum chamber. Rather than attempting to model these complex phenomena in detail, the present assessment method represents the tunnel domain boundary in this region simply as a smooth transition from flow through discrete slots to flow entering a solid wall duct. The following discussion points out several considerations which were deemed pertinent to the formulation of this simplified model of the reentry region.

Throughout the slotted test section region where measured wall pressure constraints are imposed, the streamwise flow velocity, averaged in some sense over the tunnel cross section at a given tunnel station, is firmly established by these constraints and the slot flux distribution solved to satisfy them. The velocity entering the reentry region is thereby fixed.

Let the averaged streamwise velocity entering the solid wall diffuser be constrained by one or more static pressures measured at or near this tunnel station. Because the diffuser downstream of this station is represented as a solid-wall duct with specified wall slopes, the unknown strength of the source panel at the downstream closure of the tunnel flow domain has a direct, and probably dominant, influence on satisfaction of this constraint.

Let source panels with unknown strengths be placed to cover the reentry region walls at the downstream ends of the slotted walls. In a tunnel with slotted top and bottom walls, these panels must serve in a symmetric mode to allow for mass flow conservation in the case of different streamwise velocities entering and leaving the reentry region. They must also serve in an antisymmetric mode to redirect the flow downstream of a lifting model into the direction of the tunnel axis. Stable solutions have been obtained by using pressures specified on the top, bottom and side walls to constrain the source panel strengths in the upper and lower reentry regions and the downstream closure face. Comparison of such solutions with limited actual wall pressure measurements in a reentry region, however, has raised questions about the suitability of such measured pressures for use as boundary conditions on an inviscid flow solution.

An alternate form of constraint on the reentry region source panels has evolved from consideration of the flow in the upstream portion of the slotted-wall test section. The flow velocity entering this region should be such that the most upstream pressure coefficient in each row of measured wall pressures can be matched with only a minimal disturbance at the beginning of each slot. This implies that a smoothness condition, not unlike the Kutta condition at an airfoil trailing edge, should be imposed on the slot flux development in the upstream portion of each wall slot. In the present method, this constraint is formulated to require that the line source strength gradient from the slot origin to the first strength quantifying point be equal to that between the first and second quantifying points in each slot. The region upstream of the test section is modeled as a duct with parallel solid walls in which the average streamwise velocity is firmly established by the most upstream measured wall pressures in the test section. The source panel at the upstream face of the tunnel flow domain needs to be constrained, therefore, only by the zero perturbation potential requirement on the outside flow.

Returning now to the reentry region, it has been found that a single unknown-strength source panel overlapping the most downstream segment of each slot source line provides an effective means of allowing the smoothness constraint at the upstream end of that source line to be satisfied. Conversely, because the numbers of line source quantifying points and of wall pressure constraints along each slot are equal, the added smoothness requirement at the upstream end serves to constrain the added panel source strength at the downstream end. With this arrangement, only a single measured pressure near the diffuser entrance is needed to constrain the source panel strength at the downstream closure face. In the present application, this pressure is measured on the solid side wall center line so that it is remote from the complex reentry flow.

Figure 3 demonstrates the role played in a tunnel flow solution by the interaction between the slot Kutta condition and the reentry panel source strength. These results were produced by an altered solution method in which the slot Kutta conditions were eliminated, the reentry source panel strengths were given prescribed values, and the prescription of pressure coefficient near the diffuser entrance was replaced by a prescription of a velocity entering the tunnel flow domain at the upstream face. Baseline values of the upstream velocity and the reentry source panel strengths were obtained from a solution by the unaltered solution method of a case using NTF test section dimensions, no model or sting system, and highly idealized wall pressure coefficients having a uniform value of 0.01 over the upstream portion of the slotted walls.

In figure 3a, the line plots show the slot line source strength distributions, expressed in terms of the equivalent homogeneous-wall flow angularity at the wall, and the flow angularity at the doublet panel centers on a line starting just upstream of the reentry region and extending through the reentry region and into the diffuser. For the first three cases, the flow was symmetric and results are shown only at the top wall; in the fourth case, the specified reentry panel source strengths were asymmetric and results are shown at both the top and bottom walls. Figure 3b shows the distributions along the tunnel centerline of the longitudinal velocity perturbation and flow angularity. For the first case, baseline values of the upstream velocity ($u_U = 0$) and of the top and bottom reentry source panel strengths ($F_T = 1$, $F_B = 1$) were specified and the solution, therefore, reproduced the baseline solution with essentially no disturbance at the beginning of the slots which started at tunnel station 0.16. Incrementing the upstream velocity by 0.01 (second case) caused a large outflow at the first quantifying point on each slot followed by rapidly diminishing disturbances downstream. The axial velocity diminished, accordingly, at the upstream end of the slotted test section to become stabilized at the level set by the specified slotted-wall pressures. This case demonstrates the strong link between the existence of an initial spike in the slot flux distribution and a mismatch between the upstream velocity and the specified wall pressure coefficients, implying that imposing the slot Kutta conditions should be effective in setting the upstream velocity if no conflicting constraints are imposed.

In the third case, the magnitudes of the reentry source panel strengths were increased to 1.5 times their baseline value and the additional outflow in the reentry region caused a decrease in the axial velocity entering the diffuser. There was essentially no disturbance at the upstream ends of the slots, however, because the entering velocity specification had been returned to that appropriate to the test section wall pressures. This demonstrates that

imposing the slot Kutta conditions would not impede the ability of the reentry source panel strengths to adjust to conform to an independent constraint on axial velocity entering the diffuser.

An asymmetric disturbance was introduced in the fourth case by multiplying the reentry panel source strengths by 1.5 on the bottom wall but by only 0.5 on the top wall. Because the total outflow through both walls in the reentry region was unchanged, the axial velocity distribution on the tunnel center line remained identical with that in the baseline case. A downward flow angularity is apparent, however, which exists not just in the reentry region, but over the entire length of the slotted test section. On the walls, the downwash is initiated by strong downward spikes in the slot flux on both walls and although the spikes decay rapidly, the downward flow persists over the length of the slots. It is clear that the asymmetric reentry panel strengths of this case served to turn the downward flow in the test section back to the direction of the tunnel axis in the diffuser. It is presumed at this point that if the slot Kutta conditions were restored and the reentry source panels returned to the status of problem unknowns, any downwash initiated by some independent means such as a lifting model in the test section would be cancelled by the asymmetric reentry panel strengths needed to satisfy the diffuser wall boundary conditions.

The reentry region source panel network actually used in the present method is a refinement of the single-panel-per-slot principle discussed in the preceeding paragraphs and is shown in figure 2. A single longitudinal row with an arbitrary number of panels is provided for each slot. The lateral boundaries of each row are chosen so that both the slot and its corresponding row of measured wall pressures are contained within the panel width. The source strength has a bilinear distribution over each panel and the strength at the center of each panel in a row is specified a priori relative to an arbitrary reference strength for that row. The reference strength is then used as the single unknown source strength for that row in formulating the matrix equation to be solved. This network structure allows the longitudinal distribution of source panel strength in the reentry region to be tailored empirically to fit observed characteristics of the tunnel. In the present application, the pressure distribution on the solid sidewall centerline was used as the target to be fitted.

Representation of Model and Sting. The form in which the test model and sting support are represented in the present method is identical to that of reference 14 which is, in turn, an extension of the model representation used in reference 11. In an interference assessment method, the model representation is required to yield an accurate description of the model influence at all of the problem control points which, in the present method, are on the tunnel domain boundary. Accuracy in the model near field is not required; therefore, the singularities representing the model may be discretized at low order as long as the discrete element spacing is small relative to the distance to the nearest control points. A stricter criterion should be used on the discrete element spacing for the sting because the sting influence is a part of the total interference field which is of particular interest at the model itself. The portion of the sting very close to the model, therefore, should be represented with very small element spacing.

Slender body principles are used in the representation of the model fuselage and the sting. Each is described by the axial and vertical coordinates of a series of body stations and the volumes of the body elements between adjacent stations. The influence of each element is represented as that of a source-sink pair interacting with the axial component of the onset flow and an axial doublet line interacting with the transverse component of onset flow. Added source strength may be associated with each highly inclined element by specifying the estimated width of a separated wake. The most downstream sink of a model fuselage may be omitted to represent the wake behind a blunt base and the most upstream source of a sting may be omitted to represent a sting originating within that wake.

Thin wing principles allow the influence of a wing to be represented as that of planar distributions over the wing planform of source strength to represent the thickness gradient distribution, and of vorticity to represent the lift distribution. In the present method, such distributions are presumed known for the model wing, and horizontal tail if one is present. At each of a series of spanwise stations the chordwise distribution is converted to a binomial series representing multipole singularities at the midchord, and simplified by truncating to the first four terms. The influence of these singularities is then integrated numerically across the span. The reader is directed to reference 14 for a more complete description of the model and sting representation including formulation of the multipole coefficients and of influence equations for all of the singularities.

Provision is made in the present assessment method to accept a single set of model and sting description data and apply it to multiple tunnel test points within suitable ranges of Mach number and lift coefficient. The data would include wing lift multipole coefficients for the upper and lower bounds of the lift range. Values of sting pitch setting and measured lift, drag, and pitching moment coefficients are given for each test point. The model and sting geometry is then rotated to match the pitch setting, the wing and tail lift coefficients are scaled to match the measured lift and moment coefficients while accounting for the moment contribution of the body doublet lines,

the wing lift multipole coefficients are interpolated between their upper and lower bounds, and the first order wing thickness multipole at all spanwise stations is adjusted so that the summation of induced drag and drag equivalents of wakes shed from body elements, body base and the wing trailing-edge match the specified measured drag. If a horizontal tail is not present, adjustments are made to the second order wing lift multipole coefficient to match the measured pitching moment coefficient.

It should be noted that the first and second wing lift multipole coefficients at a given spanwise station are proportional to the section lift and section pitching moment about the mid-chord, respectively. Thus, if wing lift distributions were not available from measured pressure distributions or computer solutions, wing lift data suitable for a "quick and dirty" interference assessment could be constructed from estimated spanwise shapes of wing load distribution and center of pressure location in conjunction with the known geometry and measured lift and moment coefficients.

Interference Increments and Corrections. It was noted in a previous section that after solving for the unknown panel singularity strengths, the longitudinal and vertical components of interference perturbation velocity, Δu and Δw, are calculated, both with and without sting interference, at points in the model and at other locations which may be prescribed. Because the perturbation velocities are normalized by the unperturbed reference velocity, the vertical component Δw is already in the form of an interference increment in flow angularity. Interference Mach number increments are calculated from Δu as:

$$\Delta M = \left[\frac{\left(\frac{V}{a_t}\right)^2}{1 - .2\left(\frac{V}{a_t}\right)^2} \right]^{\frac{1}{2}} - M_R \tag{2a}$$

where

$$\left(\frac{V}{a_t}\right)^2 = \frac{(1+\Delta u)^2 M_R^2}{1 + .2M_R^2} \tag{2b}$$

Interference corrections for application to model test results are determined from additional processing of the interference velocities at a set of points located in the model. The point locations are established for the particular purpose of calculating a longitudinal buoyancy correction to drag coefficient. In the model body, a pair of points is established for each element of body volume. The coordinates of the pair differ only in the longitudinal coordinates which are those of the body stations bracketing the element. The vertical coordinates are the averages of those of the bracketing body stations. Similarly, at each specified spanwise station of the wing and tail, the pair of points has the longitudinal coordinates of the leading and trailing edges of the wing or tail section and the vertical coordinates are the averages of those of the section leading and trailing edges. Static pressure coefficients are calculated from the magnitude of the interference plus reference velocity at each point and used to determine a longitudinal pressure gradient for each point pair which is multiplied by the volume of the corresponding model element to determine the longitudinal bouyancy force on that element. For the wing and tail, the element volumes are determined from the second order thickness multipole coefficients (the airfoil section areas) and the spacing of the spanwise stations. The longitudinal buoyancy correction to drag coefficient is determined from the summation of buoyancy forces on all model elements.

Interference corrections to Mach number are determined separately for the wing and tail from area-weighted averages of the interference values at the leading- and trailing-edge points.

Corrections for upwash at the wing are expressed in a form comparable to that used in the traditional wall-interference theory. At each spanwise station, the interference upwash is assumed to vary linearly between the values determined at the section leading and trailing edges. The corresponding thin-airfoil camber line has a parabolic shape with angle of attack equal to the upwash at the half-chord point. Corrections for the half-chord upwash and the camber (streamline curvature) contributions are developed separately.

The half-chord upwash distribution over the wing span leads to corrections to wing angle of attack, pitching-moment coefficient, and drag coefficient which are derived as follows. At the j-th spanwise station

$$\Delta\alpha_j = \frac{1}{2}(\Delta w_{LE} + \Delta w_{TE})_j \tag{3}$$

An effective lift slope at the j-th station, $l_{\alpha_j} = (c_{l\alpha} \cdot c \cdot \Delta y)_j$ is determined from the input values of first-order wing lift multipole coefficients given at two lift coefficients and the input angle-of-attack change between the two lift

coefficients. The wing angle of attack correction is then calculated as

$$\Delta\alpha_W = \frac{\sum_j \Delta\alpha_j l_{\alpha_j}}{\sum_j l_{\alpha_j}} \tag{4}$$

which requires no corresponding lift correction. The pitching moment caused by a nonuniform spanwise distribution of interference upwash combined with wing sweep is removed by the correction

$$\Delta C_{Mu} = \sum_j (\Delta\alpha_j - \Delta\alpha_W) l_{\alpha_j} (x_{c/4} - x_{ref})_j / S\bar{c} \tag{5}$$

The drag correction $\Delta C_{Du} = C_L \cdot \Delta\alpha_W$ accounts for rotation of the lift vector through the upwash correction angle.

Corrections to section lift and pitching moment arise from the camber (streamline curvature) contribution and are integrated over the wing span. The interference camber lift at the j-th spanwise station is evaluated by considering the change in interference upwash from the half-chord to the three-quarter-chord points as an equivalent angle-of-attack increment. Thus, the streamline curvature correction to lift coefficient is

$$\Delta C_{L,sc} = -\sum_j \frac{1}{4} (\Delta w_{TE} - \Delta w_{LE})_j l_{\alpha_j} / S \tag{6}$$

and to pitching-moment coefficient is

$$\Delta C_{m,sc} = \sum_j \frac{1}{4} (\Delta w_{TE} - \Delta w_{LE})_j l_{\alpha_j} (x_{c/2} - x_{ref}) / S\bar{c} \tag{7}$$

At the horizontal tail, a single upwash value is calculated as an area-weighted average. The difference between this value and $\Delta\alpha_W$ for the wing is reported as a correction to the tail incidence setting. All interference processing described in this section is performed on the interference velocities determined both with and without the sting influence.

Solution Smoothing and Stabilization. During development of the present method, it became apparent that use of a specified pressure coefficient boundary condition at many points on a panel network could lead to problems with solution stability. Such problems were usually in the form of divergent or anomolous spacial oscillations in the solved singularity strengths, suggesting that stabilization might be obtained through artificial smoothing. A technique is described in reference 17 for smoothing the solution of linear matrix equations addressed to problems in which the unknowns are distributed on a one-dimensional domain such as the frequency domain in spectral analysis problems. A brief summary of the technique follows.

Let the linear problem be formulated as the matrix equation

$$\mathbf{A}\mathbf{x} = \mathbf{b} \tag{8}$$

where $\mathbf{A}$ is a square coefficient matrix, $\mathbf{x}$ is the vector of unknowns, and $\mathbf{b}$ is the vector of known constants in the boundary conditions. Now, allow a family of near solutions which satisfy

$$\mathbf{A}\mathbf{x} = \mathbf{b} + \boldsymbol{\epsilon} \tag{9}$$

where $\boldsymbol{\epsilon}$ is a vector of deviations from the boundary conditions whose norm $\|\boldsymbol{\epsilon}\| = e$ is a suitably small constant. From this family, choose the solution $\mathbf{x}_s$ which minimizes the quadratic form $\mathbf{x}^{\mathrm{T}}\mathbf{C}\mathbf{x}$ where $\mathbf{C}$ is a banded matrix such that $\mathbf{C}\mathbf{x}$ is the vector of second differences expressing the smoothness of the distribution of the elements of $\mathbf{x}$ over a one-dimensional domain. Reference 17 gives the solution as

$$\mathbf{x}_s = [\mathbf{A} + \gamma(\mathbf{A}^{-1})^{\mathrm{T}}\mathbf{C}]^{-1}\mathbf{b} \tag{10}$$

where γ is a scalar multiplier which varies monotonically with the deviation norm e.

For the present problem, in which the elements of the solution vector are distributed over a two-dimensional boundary surface, the smoothing matrix C was simplified to a tridiagonal form yielding first difference smoothing, and then generalized to a two-dimensional form with the multiplier γ incorporated into the elements of C so that different amounts of smoothing can be specified in the longitudinal and transverse directions of each panel network independently. The smoothing specification for each network is contained in a square sub-matrix on the major diagonal of the C matrix. To illustrate, the sub-matrix for a simple 3 by 3 network of 9 panels takes the form:

$$\begin{bmatrix}
-f-g & f & 0 & g & 0 & 0 & 0 & 0 & 0 \\
f & -2f-g & f & 0 & g & 0 & 0 & 0 & 0 \\
0 & f & -f-g & 0 & 0 & g & 0 & 0 & 0 \\
g & 0 & 0 & -f-2g & f & 0 & g & 0 & 0 \\
0 & g & 0 & f & -2f-2g & f & 0 & g & 0 \\
0 & 0 & g & 0 & f & -f-2g & 0 & 0 & g \\
0 & 0 & 0 & g & 0 & 0 & -f-g & f & 0 \\
0 & 0 & 0 & 0 & g & 0 & f & -2f-g & f \\
0 & 0 & 0 & 0 & 0 & g & 0 & f & -f-g
\end{bmatrix}$$

where f is the smoothing factor in the direction of advancing inner index within the 3 by 3 panel array and g is the smoothing factor in the direction of advancing outer index.

Application of Method to NTF

Test Section Geometry. The physical arrangement of the NTF test section with the center line calibration probe installed is illustrated in figure 4. The divergence angle of the slotted walls δ_w about a flexible joint at station 0 is variable as are the reentry flap angle δ_f and the step height Δh at the downstream ends of the slots. The step height is controlled by varying the divergence angle of the top and bottom diffuser walls about a joint at station 11.28.

Pressure orifices were installed directly into the test section walls in nine longitudinal rows, three each in the top, bottom and one of the side walls. On the slotted top and bottom walls, the orifice rows were located halfway between slots on the center wall slat and on the next two slats toward the instrumented side wall. On the side wall, orifice rows were located at the center line and the one-quarter and three-quarter height locations. The two off-center rows on the sidewall were not used in the assessment method. The orifice rows on the slotted walls extended between stations 0.3 and 6.75, and that on the sidewall centerline extended downstream to station 8.13. Orifice spacing varied from 7.6 cm in the central region of the test section to as much as 30 cm elsewhere.

The paneling distribution used to model the NTF test section was the same as that shown on figures 1 and 2. The lateral location of the pressure coefficient control points in the NTF model, however, was halfway between slots to conform to the orifice row locations. The assessment problem for the NTF test section solved for 581 unknown singularity strengths to satisfy 496 zero perturbation constraints on the exterior flow, 79 pressure coefficient specifications, and six slot Kutta conditions.

Refinement of Reentry Region Model. In a foregoing section describing representation of the reentry region, it was noted that the shape of the longitudinal distribution of panel source strength would be tailored empirically with matching of the observed pressure distribution on the solid sidewall centerline as a target. This tailoring was accomplished as follows.

Let a longitudinal coordinate in the reentry region be defined as

$$X = \frac{x - x_U}{x_D - x_U} \tag{11}$$

where x_U and x_D are the tunnel stations at the upstream and downstream ends, respectively, of the reentry region. Now, express the source strength σ at panel centers as

$$\sigma_{ij} = \Sigma_i \cdot s(X_j) \tag{12}$$

where Σ_i is the unknown reference strength for the i-th row, and $s(X)$ is a shape function applicable to all rows. A discrete value of $s(X)$ is specified at each panel center location X_j of the j-th panel in any row.

To illustrate the effect on the sidewall centerline of changing the shape function $s(X)$, the upper part of figure 5 compares the calculated pressure coefficient distributions on the sidewall centerline from the present method using constant, linear, and parabolic reentry shape functions. The test case illustrated was for a Mach number of 0.8 with the calibration probe installed as shown in figure 4. The sidewall centerline pressure at tunnel station 7.05 was specified to control the velocity leaving the reentry region but the calculated pressures at all other sidewall locations were free to respond to the changes in the reentry shape function. In the lower part of figure 5 the calculated distribution for $s = X^2$ is compared with the pressure coefficients actually measured at the sidewall pressure orifices and the agreement is better than it would be with the constant or linear shape functions. The shape function has been generalized to a one-parameter family of second-degree functions which satisfy

$$s = \begin{cases} 0, & \text{if } X = 0 \\ q, & \text{if } X = .5 \\ 1, & \text{if } X = 1 \end{cases} \tag{13}$$

and can be expressed as

$$s = (4q - 1)X + (2 - 4q)X^2 \tag{14}$$

The linear and parabolic functions used for figure 5 are members of this family having values of q of 0.5 and 0.25 respectively. Examination of the results of using this family with NTF calibration points with varying Mach number, Reynolds number and test section geometry settings have shown the agreement between calculated and measured sidewall pressure distributions is generally good if the parameter q is varied only with Mach number. The empirically derived schedule

$$q = 0.1557 + 0.4715\left(1 - \sqrt{1 - M^2}\right) \tag{15}$$

has been found to yield satisfactory results over a wide range of test conditions both with and without a test model.

Test Data Preprocessing. The present interference assessment method is embodied in a computer program which resulted from augmenting and specializing a general purpose panel method program. The input data required by the program falls into three categories: (1) data applicable to most tests in a given wind tunnel, (2) data applicable to the particular test model configuration and installation, and (3) data applicable only to a single test point.

Because manual preparation of the input data for more than one or two test points can be tedious and time consuming, a system of utility computer programs has been developed to aid the application of the present method to the NTF. The first input data category consists primarily of geometric definition of the tunnel paneling, pressure control point locations, and boundary condition types. This part of the input data was evolved for the NTF during development of the assessment program and should change only rarely. Computer assistance in preparing the model representation data of the second category is provided by a transonic small disturbance equation code for aircraft configuration analysis which has been augmented to perform the chordwise integration of both the thickness and lift distributions over the model wing and tail needed to determine the multipole series coefficients used by the present method, as well as to translate the fuselage geometry description into the form required. The work of J. A. Al-Saadi at NASA Langley Research Center in augmenting the transonic analysis code is hereby acknowledged. He found that the interference assessment results were sufficiently insensitive to changes in wing lift distribution that suitable model representation over a test series on a transport aircraft model could be obtained from multipole coefficients for a small number of Mach number, angle-of-attack combinations.

Particular attention has been paid to automating the preparation of the case-dependent data in the third category and its assembly into an input data file for interference assessment of multiple test points. It has been found that a necessary task in the data processing stream is smoothing of the pressure coefficient distribution along each longitudinal row of wall pressure orifices. The scatter in the individual measured pressures in each row is sufficient to impact adversely the accuracy of the assessed interference results. The pattern of the scatter in any row, however, is sufficiently consistent over a large group of test points to imply that it arises from geometric imperfections in the shape of the installed orifice and the nearby wall region. The potential exists, therefore, to improve the quality of the measured wall pressure data by imposing corrections based on a fixed, empirically derived array of some form of correction parameter. Because the magnitude of the scatter pattern is apparently dependent on test conditions, including Reynolds number, development of such a correction array is not straightforward. For the present, an array of default values of orifice weighting factors for the data smoothing process is used and is being refined with continuing accumulated experience.

Case-dependent data processing begins with transfer of the array of wall pressure coefficients and values of sting pitch setting, test section geometry settings, lift, drag, and pitching-moment coefficients, and test point identification data from the regular NTF data reduction output to a standardized format file in which, for each test point, the wall pressures are organized into rows and augmented by the default array of orifice weighting factors and row smoothing parameters. A wall pressure editing utility may then be used in a batch mode to produce plots showing the pressure coefficient data, weighting factors and the resulting smoothed distribution for all rows for all or specified test points. These plots may be scanned rapidly to find occurrences of bad data and to judge the suitability of the weighting and smoothing factors. The editing utility also may be used interactively for an individual row and test point to alter one or more weighting factors or the smoothing parameter, immediately display the new smoothed distribution, and save the alterations in the data file. Finally, another utility assembles multiple-case input data files starting with the previously prepared files with category 1 and 2 data and appending multiple case-dependent data in which the wall pressure coefficients are smoothed using the current smoothing parameters for the appropriate test point and interpolated to the appropriate control point locations. The author wishes to acknowledge the valuable work of A. B. Graham of Unisys Corp. and N. T. Frink of NASA Langley Research Center in developing the wall pressure plotting, editing, and smoothing utilities and the file format with which they operate.

Interference Assessment Results in NTF

Results are presented in this section of interference assessment of selected test points from NTF test section calibration tests using the centerline probe installation sketched in figure 4, and from tests of two subsonic transport configuration models in the NTF. All of the results were produced by the assessment method of this paper using as wall pressure boundary conditions, the static pressures measured at orifices installed directly in the test section walls and reduced to coefficient form without subtraction of any "empty tunnel" tare pressures. The static pressure in the plenum chamber surrounding the slotted-wall test section was used as the pressure coefficient reference for all tests except those of the second transport model for which a tunnel calibration correction, determined from the calibration tests as a function of Mach and Reynolds numbers, was applied to the reference conditions. All results shown are for a Mach number of 0.8, a reentry flap setting δ_f of 0 deg., and a reentry step height Δh of 0.13m unless otherwise noted. Note that values of Reynolds number cited herein as R_u are unit Reynolds numbers based on a length unit of $0.1\sqrt{C}$ where C is the cross section area of the test section. This form has been used to correlate properties of the wind tunnel rather than properties of the model under test.

Tunnel Calibration Tests

The present interference assessment method calculates first a tunnel flow field which is required to satisfy all boundary conditions including those imposed as measured wall pressure coefficients, then a total interference field which is the summed influence of all singularities except those representing the test model, and a wall interference field which omits the influence of singularities representing both the model and the sting. It is of interest to examine first the fidelity with which the calculated tunnel flow field reproduces that which actually existed during the test. The tests of the centerline probe used for tunnel calibration and shown in figure 4 are useful for this purpose. Figure 6 shows the pressure distribution calculated on the surface of the centerline probe compared with the pressure coefficients actually measured on the probe during three tunnel calibration test points with different wall divergence settings. Of course, these measured pressures were not used as boundary conditions on the calculation. Upstream of station 0, the calculated and measured results differ because the tunnel contraction region was modeled in the assessment method as a simple parallel-wall duct. The measured pressure increments in this region due to changing test section wall divergence, however, are well matched by those in the calculated levels. At stations within the test section, the calculated pressures lie within the scatter band of the measured pressures but are generally near the positive pressure edge of the scatter band. The positive pressure trend approaching the start of the flared probe support at station 5.49 is well matched by the calculated results.

The pressure orifice row on the centerline of the solid test section sidewall offers another opportunity to judge the fidelity of the tunnel flow solution. Only a single value of measured pressure coefficient from this row, that at station 7.05, was enforced as a boundary value for the solution. In figure 7, the measured and calculated pressure distributions on this row are compared for the same test points for which the probe pressures are shown in figure 6. The suction peak just downstream of station 7.62 arises from the bend in the sidewall at the entry to the solid-wall diffuser. An effective inviscid shape of this bend was derived from a pressure distribution similar to those shown and has been used as an invariant shape for all subsequent assessment runs. The pressure distribution in the reentry region, stations 6.10 to 7.62, is seen from figure 7 to vary greatly with changes in wall divergence but the good

agreement between the calculated and measured distributions here attests to the effectiveness of the slotted-wall reentry region model used in the present method. Through the slotted-wall part of the test section, the calculated pressures again lie within the scatter band of the measured data but appear to be slightly less positive than a well-smoothed curve through the data would be.

Figure 8 shows the effect of variations in Reynolds number on the comparison of calculated and measured wall pressures on the sidewall centerline row of orifices. The scatter in the measured data clearly increases with increasing Reynolds number, probably because at low Reynolds number, the flow disturbances arising from shape imperfections of an orifice or of the wall close to an orifice are attenuated by a thicker boundary layer than at high Reynolds number. The calculated pressure distributions through the slotted-wall part of the test section depend primarily on the pressure boundary conditions on the top and bottom (slotted) walls which were quantified by a computerized smoothing routine acting on the pressure measurements at the discrete orifice locations. The top and bottom wall pressure measurements exhibited an increased scatter with increasing Reynolds number similar to that shown for the sidewall pressures which implies that the accuracy of assessment results might also decrease with increasing Reynolds number.

Considering all of the comparisons given in figures 6 to 8, the pressure coefficients in the calculated tunnel flow in the vicinity of the nominal model location at station 3.96 apparently agree with those in the actual flow within about 0.004 which corresponds to an accuracy in velocity or Mach number of about 0.2 percent. The fidelity of the calculated tunnel flow with respect to flow angularity is discussed in a subsequent section of this paper in the context of tunnel interference at a test model.

In applying the present assessment method to the NTF calibration tests, the entity identified as the test model was the centerline probe itself which, as shown in figure 4, extended from the probe nose, well upstream of the test section origin, to the intersection of the cylindrical probe surface with the conical surface of the flared probe support at station 5.49. From this point downstream, the probe support is identified to the assessment method as a model support sting. The singularities representing the test model are simply the small sources at the probe nose and have little influence on the flow within the test section. The assessed total interference field is, therefore, essentially the field of empty tunnel flow perturbations from the uniform reference flow at a velocity corresponding to the plenum chamber static pressure.

Surveys through the calibration test interference field are given herein to demonstrate the NTF test section flow properties, particularly as affected by the controllable geometry features shown on figure 4, the top and bottom wall divergence, δ_w, the reentry flap setting, δ_f, and the reentry step height, Δh. A longitudinal survey line located at $y = .625$m, $z = 0$, so as to lie halfway between the tunnel axis and the centerline of the test section sidewall, is chosen to illustrate the longitudinal distribution of flow through the entire length of the test section without being unduly influenced by effects of either the flared probe support on the tunnel axis or the bend in the sidewall at the downstream end of the reentry region.

In figure 9, the distribution of the total interference Mach increment along this survey line is shown for a range of wall divergence settings from -0.3 ° (top and bottom walls converged) to 0.19 ° (walls diverged). In the slotted-wall part of the test section, the level of ΔM_{tot} becomes more negative as the wall settings vary from diverged to converged. Near tunnel station zero, the ΔM_{tot} change with wall setting is exaggerated by the flow adjustment from the nozzle which ends with parallel walls to the test section which might have sloped top and bottom walls. Because the reference flow has a static pressure equal to the plenum pressure, the level of the negative interference Mach increment is an indicator of the pressure difference across the walls which causes the flow to curve outward through the wall slots. In the reentry region downstream of station 6.10, the trend of ΔM_{tot} with wall setting is reversed. In this region, any flow which has left the test section through the slots must be reintroduced to enter the solid-wall diffuser. The flow quantity thus exchanged is greatest for the converged wall settings which also give the smallest tunnel cross section area at the diffuser entrance resulting in the highest velocity in the reentry region.

An important use of the calibration test results is to select optimal wall settings for each Mach and Reynolds number condition. For the NTF, the goal was to minimize the longitudinal pressure (or Mach) gradient measured on the probe surface between tunnel stations 3.05 and 4.88. This region brackets the nominal model location at station 3.96. For the conditions of figure 9, a converged wall setting of -0.11 °, met this criterion. Although the ΔM_{tot} distributions of figure 9 are on a survey line displaced laterally from the probe, it is apparent that the probe support flare, starting at station 5.49, probably influences the pressure gradient used as a criterion. In figure 10 the interference Mach increment evaluated without sting influence (i.e. without the influence of the flared probe support) is shown for the same conditions as those of figure 9. The resulting ΔM_{wall} distributions flow more smoothly from the slotted test section through the reentry region into the diffuser than do the ΔM_{tot} of the previous figure. In the criterion region between stations 3.05 and 4.88, the diverged wall setting of 0.19 ° now shows a small gradient as well

as a small value of ΔM_{wall}. Apparently, this divergence of the top and bottom walls approximately compensates for the boundary layer growth on all four tunnel walls so that little slot flux is required. These results illustrate the usefulness of the present assessment method for identifying the source of tunnel flow perturbations even without a test model installed. In particular, the choice of a wall setting to produce zero pressure gradient on the calibration probe now can be recognized as including compensation for the flared probe support in both the Mach calibration value and its longitudinal gradient. This wall setting choice need not be deemed inappropriate because the sting support system for a typical model test in NTF will probably produce interference effects similar to those of the calibration probe support.

The effects on the ΔM_{wall} distribution of varying the reentry flap setting are illustrated in figure 11. At negative settings of δ_f, the flap leading edge, located at station 6.10, lies closest to the slotted-wall surface, effectively narrowing the entrance to the diffuser and causing a local region of high velocity. The perturbations due to varying δ_f propagate upstream from the reentry region and are felt at the nominal model location as changes in longitudinal Mach gradient. The flow at the upstream end of the test section is not affected by the reentry flap setting. As shown in figure 12, the effects of varying the step height at the downstream end of the reentry region are similar to those of varying the reentry flap setting but do not propagate as far upstream and have practically no effect at the nominal model location.

The question of consistency of interference assessment results over time is addressed in figure 13 where assessment results from a tunnel calibration test run in early 1987 are compared with similar results from an early 1990 test. Although the two test programs did not include identical wall divergence settings, the ΔM_{tot} results shown in figure 13a for a range of δ_w settings shows that results from both test programs merge into a consistent trend. The upwash component of interference, $\Delta\alpha_{tot}$, ideally should be zero because of the symmetric geometry of the test section with the calibration probe installed. Figure 13b shows, however, that for the 1987 test, the assessments produced negative values of $\Delta\alpha_{tot}$ over the entire length of the test section with a minimum value of about $-0.12\,^\circ$ occurring near the nominal model location. For the 1990 test the assessed upwash interference was much closer to zero. Within a given test year, little variation of $\Delta\alpha_{tot}$ with wall divergence setting is observed. Further discussion and interpretation of assessed upwash interference is given in a subsequent section of this paper where results from model tests are included.

Tests of Subsonic Transport Models

The NASA Langley Research Center Pathfinder I Model. The present interference assessment method has been applied to tests in the NTF of two models of different subsonic transport aircraft configurations. The first is the Pathfinder I (PF1), a model which has a generic subsonic transport configuration and was developed at NASA Langley Research Center for the purpose of gaining experience with the new model design, construction, instrumentation and testing techniques compatible with the cryogenic test environment of the NTF. The results presented herein were drawn from a test program conducted in mid-1987 at which time some problems existed with the NTF wall pressure instrumentation electronics, requiring that significant manual effort be invested in examining, weighting, and smoothing the pressure data for each test point to be assessed. The number of test points assessed was, therefore, relatively small.

A drawing of the Pathfinder I model and the forward part of its model support sting is shown in figure 14. The model span was 54 percent of the test section width and the frontal area of the model blocked 0.62 percent of the tunnel cross section area. The Pathfinder I support sting emerged from the blunt model base with a diameter smaller than the model base diameter. At small angles of attack, the part of the sting closest to the model would be expected to remain immersed in the wake behind the model base and, therefore, have little effect on the flow outside of the wake. Because the interference assessment program uses inviscid aerodynamics, however, the input to the program defined the model and sting singularities in such a way as to reflect this wake effect. A wake was assumed to trail from the model base with a constant displacement cross section equal to that of the model base. The part of the sting from the model base to a point 22.6 cm downstream of the base (shown dashed in figure 14) was omitted; downstream of this point, the sting was described in its true geometry but the source representing a blunt upstream sting face was suppressed so that only the growth of cross section area from this point downstream was represented.

Contour plots in the wing reference plane of total interference increments in both Mach and upwash angle are shown in figure 15 superimposed on the Pathfinder I planform for a typical test point with moderate lift. This form of presentation is useful for conveying a quick impression of the variability of the interference field over the model planform. Note, for example, the high density of the ΔM_{tot} contours over the horizontal tail where the Mach number is being depressed as the sting is approached.

The form of presentation illustrated in figure 16 includes all of the corrections to the model test data for a given pitch run, calculated from the total interference field by the procedures described in a previous section of this paper. The corrections given in figure 16 are for a typical run of the Pathfinder I model with a horizontal tail at Mach 0.8 and a low Reynolds number. Values of ΔM_{tot} are given as averaged over both the wing and the tail planforms. The wing value is probably most appropriate to use as the Mach correction for each test point while the tail value might be used to adjust derived characteristics such as tail effectiveness. The upwash correction given for the wing, $\Delta\alpha_W$, is intended for application as a correction to model angle of attack. The interference upwash averaged over the tail usually has a value different from $\Delta\alpha_W$ and that difference is shown as a correction to the tail incidence setting. The upwash interference at the wing is negative at zero lift with a hint of positive gradient with lift coefficient. At the tail, the additional upwash interference clearly shows a positive gradient with lift.

In figure 17 the corrections are given as evaluated from the wall interference field with the sting contributions omitted. Although these results are not appropriate for actual corrections to the model data, they may be compared to those of figure 16 to illustrate the effects of sting interference. It is seen that the sting effect causes a negative increment in Mach interference, particularly at the tail, and the corresponding change in Mach gradient caused a significant change (about seven counts) in the buoyancy correction to drag coefficient. The remaining corrections arise from interference upwash and its distribution and show practically no contribution from sting effects.

The Boeing Commercial Airplane Company 767 Model. The Boeing 767 model (B767) was tested in NTF in late 1988 to allow comparison of NTF test data with data from the same model in other tunnels and with flight and tunnel data on the same configuration. The NTF wall pressure instrumentation was upgraded prior to this test and was monitored carefully and calibrated frequently during the test. In subsequent processing of the wall pressure data, a default set of orifice weighting factors and row smoothing factors was evolved which then permitted acceptable smoothing of the data with only a small amount of human intervention. The assessment program was applied to many pitch runs with about eight points per run being assessed. The results presented herein are a very small sample selected to illustrate the major findings of the interference assessment study of the B767 model test.

A drawing of the B767 model and the forward part of its support system is shown in figure 18. The model span was 57 percent of the test section width and the frontal area of the model blocked 0.84 percent of the tunnel cross section area if nacelles and pylons were installed. The model support sting system consisted of a swept strut which emerged from the fuselage at a location roughly equivalent to that of a vertical tail, and merged with a circular cross section sting which was above and parallel to the longitudinal body axis of the model. Farther downstream, this sting was fastened to the NTF sting system at such an angle that the model reference point was at the sting center of rotation at tunnel station 3.96. The swept strut support has the advantage that the geometry of the fuselage and horizontal tail need not be distorted to accommodate the model support.

As noted in a foregoing section of this paper, a support sting is represented in the present assessment method as a series of segments, each being modeled with a source-sink pair and a line doublet segment. To apply this representation to the B767 support, the portion of the swept strut and sting external to the model was cut by a series of planes normal to the longitudinal body axis and the centroids of the cross sections thus defined were used as the segmented sting stations with the volume of each segment specified as the exposed strut volume between adjacent cutting planes. The locus of the resulting sting segment axes is shown as a dashed line in figure 18. No part of this swept strut and sting was assumed to be shielded by a viscous wake.

Total interference corrections are given in figure 19 for a pitch run of the B767 model without a horizontal tail at Mach 0.8 and a Reynolds number of 6.1×10^6. The data reduction procedure for the B767 test program included a tunnel calibration correction to the reference Mach number which was accounted for in all data including the wall pressure coefficients. For the test conditions of figure 19 this correction was -.0039. The figure shows, however, that an additional Mach correction for total interference of -.004 or more is needed. Furthermore, the buoyancy correction to drag coefficient varies significantly with lift coefficient, whereas no such trend was apparent with the Pathfinder I model. The corrections calculated with the sting contribution omitted, shown in figure 20, indicate a near zero ΔM at the wing (at least at low lift) and a nearly constant buoyancy correction to drag coefficient which imply that the sting contribution to Mach interference is indeed large, even at the wing, and imposes perturbations on the model fuselage which vary with angle of attack. The sting also contributes a downwash increment at the wing which was not the case with the Pathfinder I.

Interference corrections for a run at the same test conditions of the complete B767 configuration including a horizontal tail are shown with the sting effects included and omitted in figures 21 and 22, respectively. The corrections given previously for the model without horizontal tail were not affected significantly by addition of the tail. With sting effects omitted (fig. 22), the longitudinal gradient in ΔM_{wall} is apparent in the more positive values

given at the tail than at the wing as was the case for the PF1 model. With the B767 sting effects included (fig. 21), the values of ΔM_{tot} remained more positive at the tail than at the wing except at the highest angles of attack, and the sting effects shifted the tail incidence correction negatively by about 0.3 degrees. Two properties of the B767 support system contribute to these results; first, some of the growth of cross section area blocking the flow occurs upstream of and above the tail plane, and second, the crossflow around the swept strut section (modeled by the line doublet segments) induces downstream and downward velocity components outboard of the swept strut. This second effect is probably exaggerated somewhat because the swept strut is modeled as an inclined body of revolution rather than as a swept thick airfoil.

The B767 test program included tests at three different values of R_u ranging from 6.1×10^6 to 55.1×10^6. All of the B767 corrections presented to this point were from tests at the lowest Reynolds number. Variations in Reynolds number had only minor effects on all of the corrections except the upwash correction at the wing. Figure 23 shows the correction $\Delta\alpha_{W,wall}$ assessed from a typical pitch run at each of the three test Reynolds numbers. Included for comparison are values of tunnel flow angularity evaluated by traditional methods from model erect and inverted tests and plotted at zero lift. Each such point plotted is the average of several such evaluations at the same Reynolds number. Because both the sting and the model were inverted together for the traditional evaluations, it is appropriate to compare these results with assessed results evaluated with the sting contribution omitted.

It is apparent from figure 23 that the assessed upwash correction at the wing near zero lift varied by about 0.2 ° from the lowest to the highest test Reynolds number whereas that determined from model erect and inverted tests varied by only about 0.03 ° over the same range. Furthermore, the negative assessed values of $\Delta\alpha_W$ shown in foregoing figures for tests at low Reynolds number are not supported by the flow angularity results from model erect and inverted tests. One suggested source of error in the assessed results might be the existence of a Reynolds number dependent angularity in the flow emerging from the entrance nozzle upstream of the NTF test section. In the assessment method, this upstream flow is guided by parallel solid walls assumed to have zero slope. In the test section, the flow upwash at a given station is strongly influenced by the longitudinal integration from the upstream flow to the station in question, of the measured (and smoothed) pressure difference between the top and bottom walls; but, at the same time, the test section flow must satisfy the Neumann condition imposed on the flats between slots. Experimentation with the assessment program has indicated that a change in flow angle upstream of the test section entrance, produced by changing the upstream wall slopes, decreases in the vicinity of the test section entrance to an increment less than half of the upstream slope change. This implies that the upstream flow angularity would have to change more than 0.4 ° over the Reynolds number range to produce the effects shown on figure 23.

In an attempt to gain more insight into the behavior of these assessed Reynolds number effects, the longitudinal distribution of the assessed interference components along the survey line halfway between the tunnel axis and the sidewall centerline have been evaluated for four of the test points shown on figure 23, those at the lowest and highest Reynolds numbers at lift coefficients closest to zero and 0.56. The distributions of ΔM_{wall} are given on figure 24a and show that over most of the test section length, essentially no effect of changes in Reynolds number or model lift is seen. The differences existing near station zero and in the reentry region arise primarily from the difference in wall divergence settings chosen from the calibration tests for the two Reynolds numbers. The values of δ_w for the lowest and highest Reynolds numbers were -0.11 ° and +0.03 °, respectively. The longitudinal distributions of $\Delta\alpha_{wall}$ for the same four test points are given on figure 24b. At each Reynolds number, the effect of increasing lift coefficient is to cause a positive increment in $\Delta\alpha_{wall}$ which grows from zero just upstream of the model location to about 0.4 ° at the downstream end of the reentry region. The effect of increasing Reynolds number, however, starts immediately downstream of the slot origin station and is apparent throughout the length of the slotted wall and reentry region.

At a given model lift coefficient, the only differences between the assessment input data sets for different test Reynolds numbers occur in the values of measured wall pressure coefficient specified as boundary conditions. The pressure coefficients measured by the three orifice rows on each of the bottom and top walls for the test point at R_u of 6.1×10^6 and C_L of 0.569 are shown in figure 25a and the corresponding data at R_u of 55.1×10^6 and C_L of 0.551 are shown in figure 25b. In each figure, the individual orifice C_p values are shown by symbols and the smoothed distributions from which boundary condition values were picked are shown by faired lines. Distributions on the bottom and top walls at the same lateral location are superimposed on the same plot so that the pressure difference between bottom and top walls can be seen directly.

The effect of the lifting model and its wake is readily apparent in the pressure difference between bottom and top walls starting about tunnel station 3. This difference peaks at about station 4 where figure 24b shows a rapid upward curvature in $\Delta\alpha_{wall}$ for the two higher lift cases. One might expect to find similar evidence in the wall pressure differences relating to the upward curvature at tunnel station 1 for the high Reynolds number case but it is not as readily apparent. On figure 25 the pressure distributions upstream of tunnel station 3 for the wall centerline

rows ($y = 0$) appear to be relatively uniform with very small pressure differences between the bottom and top walls at either Reynolds number. The pressure data at the two other lateral locations show generally more scatter and the occurrence of unexpected nonuniformities near the upstream end of the test section. Because the most upstream wall pressure control points used in the assessment solution are at tunnel station 0.85, the full impact of these upstream nonuniformities is avoided. It should be noted that the orifice rows on the centerline of each wall ($y = 0$) were installed before the final machining of the wall surface whereas the two off-center rows were installed later using methods more likely to cause surface shape imperfections. At the lower Reynolds number, the two off-center pressure rows show top wall pressures that are slightly more positive than those on the bottom wall between stations 0.85 and 3.0; whereas at the higher Reynolds number this pressure difference between walls is generally reversed. This observation is consistent with the Reynolds number effects on $\Delta\alpha_{wall}$ shown on figure 24. It is suggested that the Reynolds number effect on the measured wall pressures might be associated with the interaction between wall shape imperfections near the pressure orifices and the thinning of the wall boundary layer with increasing Reynolds number.

It is concluded from the foregoing discussions that inherent difficulties exist in obtaining consistent and accurate values of the upwash component of wall interference from the present assessment method applied to the NTF with the present wall pressure instrumentation. The assessed upwash interference at the model wing differs by 0.2 ° between the lowest and highest Reynolds number tests of the B767 model. Although all of the information needed to predict this change is contained in the measured wall pressures, the Reynolds number effect on wall pressures is almost obscured by the scatter in the pressure data. Furthermore, the responsible pressure change originates well upstream of the model wing and the effect on upwash at the wing is accumulated through a longitudinal integration process. In contrast, the assessed Mach (longitudinal velocity) interference is controlled by an effective average of the wall pressures in the immediate vicinity of the tunnel station in question and shows much better consistency than the assessed upwash. An additional source of upwash error could arise from the assumption of zero angularity in the flow upstream of the test section. The existence of non-zero flow angularity upstream would affect the comparison of the assessed upwash at the model with the upwash deduced from model erect and inverted tests (as in figure 24). A related phenomenon is the possible change in the tunnel flow pattern with time. A difference of about 0.1 ° is shown in figure 13 between the upwash values assessed from tunnel calibration tests run in 1987 and 1990. The earlier result appears reasonably consistent with the low Reynolds number results assessed from tests of the PF1 and B767 models. It is interesting to note that flow angularity values obtained from model erect and inverted tests of a model which was tested shortly after the 1990 calibration test were greater than 0.1 ° whereas values of 0.03 to 0.06 are shown on figure 23 for the B767 test. The assessment method has not been applied to this later model test.

NTF Blockage Characteristics. On the lower part of figure 26, the distributions of ΔM_{wall} on the survey line halfway between the tunnel axis and the sidewall centerline assessed from selected test points near zero lift from the PF1 and the B767 model tests are compared with distributions from the calibration probe test selected to have R_u values of the same order and comparable wall divergence settings. For the B767 assessments shown in this figure, the wall pressure coefficients were recalculated to use plenum pressure as the coefficient reference for comparability with the other tests. It is apparent that the distributions from the tests of either model have a less uniform slope through the slotted portion of the test section than do those from the calibration probe tests. The model test distributions are characterized by a slight peak centered in the region occupied by the model and a minimum upstream of the model. It is suspected, however, that discrepancies exist in the level of ΔM_{wall} such that the comparison between individual distributions is not always consistent with the trends with wall divergence or Reynolds number presented in foregoing figures. Such inconsistencies apparently approach values of as much as ± 0.001.

The upper part of figure 26 shows theoretically predicted solid blockage ΔM distributions taken from results presented in reference 14 and scaled to the volume of the B767 model in the NTF test section for Mach 0.8. Results are presented for solid tunnel walls and for the NTF walls represented as finite-length slotted top and bottom walls having a homogeneous ideal slotted-wall parameter, K, of 3.0 with nonlinear inflow and outflow terms included. The theoretical solid blockage Mach increment is predicted to be only 0.005 for this size model even in a solid-wall test section and is predicted to be much less in the NTF slotted test section. Of course, the theoretical blockage interference is an example of wall interference under the traditional interpretation as interference arising only from interaction of the walls with the model-induced perturbation field. Values of ΔM_{wall} from the assessment program, on the other hand, include not only the model-wall interaction but also any perturbations from the reference Mach number contained in the empty tunnel flow. To the extent that these empty tunnel perturbations are represented by the assessment results from the calibration probe tests, the distributions of ΔM_{theo} should be compared with the difference between assessed ΔM_{wall} distributions from the model and probe tests. It is clear that the slope

variations contained in the assessed model test distributions are indeed similar to those in the ΔM_{theo} distribution predicted for the NTF slotted walls even though the aforementioned discrepancies in level of ΔM_{wall} exceed in some cases the magnitude of the theoretical interference.

Concluding Remarks

A method for assessing the interference existing in tests in a slotted-wall wind tunnel and quantifying corrections to the test data has been described. In the method, the tunnel walls are modeled by a high order panel method augmented by special features to represent finite-length discrete wall slots and to approximate the effects of a complex flow in a reentry region terminating the downstream ends of the slots. Mixed boundary conditions enforce satisfaction of both the tunnel geometry and wall pressure distributions measured in the slotted-wall region. The test model is represented by distributed singularities with strengths specified so as to match the test values of lift, drag, and pitching-moment coefficients. Other specified-strength singularities may be used to represent a model support sting system.

The interference field described by the assessment method includes not only the traditional wall interference phenomena which arise from interaction of the tunnel walls with model-induced perturbations, but also any perturbations from a uniform reference flow resulting from the tunnel walls and the model support sting. The corrections to model data calculated by the method should, therefore, be considered as equivalent to the summation of traditional corrections for tunnel Mach calibration, longitudinal pressure gradient, tunnel flow angularity, wall interference, and an inviscid form of sting interference. An alternative form which omits the direct contribution of the sting from both the interference field and the corrections is also included in the output of the assessment method.

The method of this paper has been applied to the National Transonic Facility (NTF) at NASA Langley Research Center for tunnel calibration tests as well as tests of two models of subsonic transport configurations. Assessment of the calibration test results was found useful to demonstrate the effects of variable test section geometry features. It was shown that the selection of a wall divergence setting to achieve zero longitudinal Mach number gradient at the nominal model location was significantly affected by the existence of a flared support for the calibration probe.

Accuracy of the assessment results was found to be limited by scatter in the wall pressure data caused primarily by imperfections in the wall orifice installation and influenced by Reynolds number effects on the wall boundary layer thickness. Resulting inconsistencies in the components of assessed interference were observed to be as high as ± 0.001 in Mach number and $\pm 0.1^\circ$ in flow angle. These inconsistencies were larger in magnitude than the wall interference predicted by traditional methods for the two transport models but trends characteristic of the traditional wall interference could be detected in the assessed results. The sizes of the two models were conventional for high subsonic speed tests, with wing spans of 54 and 57 percent of the tunnel width and frontal areas of 0.62 and 0.84 percent of the tunnel cross section area.

The possibility of improving assessment accuracy by using wall pressure differences between model-installed and model-removed tests as assessed boundary conditions was not examined because tests have not been conducted with either of the model support systems installed but without the model.

Significant levels of support interference were shown by the assessment results for one model having an upper swept strut support attached to a displaced sting. The sting effects for the other model which was supported by a sting emerging symmetrically from the blunt model base was limited to modest changes in blockage and longitudinal buoyancy interference.

References

1. Murman, Earll M.; and Cole, Julian D.: *Calculation of Plane Steady Transonic Flows.* AIAA J., vol. 9, Jan. 1971, pp. 114-121.
2. Ferri, A.; and Baronti, P.: *A Method for Transonic Wind-Tunnel Corrections.* AIAA J., vol. 11, Jan. 1973, pp. 63-66.
3. Sears, W. R.: *Self Correcting Wind Tunnels.* The Aeronautical J., vol. 78, Feb./Mar. 1974, pp. 80-89.
4. Berndt, S. B.; and Sorensen, H.: *Flow Properties of Slotted Walls for Transonic Test Sections.* AGARD-CP-174, Oct. 1975, Paper no. 17.
5. Berndt, S. B.: *Inviscid Theory of Wall Interference in Slotted Test Sections.* AIAA J., vol. 15, Sept. 1977, pp. 1278-1287.
6. Agrell, N.; Pettersson, B.; and Sedin, Y. C-J.: *Numerical Computations and Measurements of Transonic Flow in a Slotted-Wall Wind Tunnel.* AIAA Paper no. 87-2610, Aug. 1987.

7. Kraft, E. M.; Ritter, A.; and Laster, M. L.: *Advances at AEDC in Treating Transonic Wind Tunnel Wall Interference.* 15th Congress, International Council of the Aeronautical Sciences, London, U.K., Sept. 7-12, 1986. Proceedings, vol. 2, 1986, pp. 748-769 (ICAS-86-1.6.1).
8. Tuttle, M. H.; and Mineck, R. E.: *Adaptive Wall Wind Tunnels - A Selected, Annotated Bibliography.* NASA TM-87639, Aug. 1986.
9. Newman, P. A.; Kemp, W. B., Jr.; and Garriz J. A.: *Emerging Technology for Transonic Wind-Tunnel-Wall Interference Assessment and Corrections.* SAE Technical Paper 881454, Oct. 1988.
10. Kemp, W. B., Jr.: *TWINTN4: A Program for Transonic Four-Wall Interference Assessment In Two-Dimensional Wind Tunnels.* NASA CR-3777, Feb. 1984.
11. Rizk, M. H.; and Smithmeyer, M. G.: *Wind-Tunnel Wall Interference Corrections for Three-Dimensional Flows.* J. Airc., vol 19, June 1982, pp. 465-472.
12. Mokry, M.; Digney, J. R.; and Poole, R. J. D.: *Analysis of Wind Tunnel Corrections for Half Model Tests of a Transport Aircraft Using a Doublet Panel Method.* 15th Congress, International Council of the Aeronautical Sciences, London, U.K., Sept. 7-12, 1986. Proceedings, vol. 2, 1986, pp. 779-785. Also: J.Airc., vol. 24, May 1987, pp. 322-327.
13. Rizk, M. H.; and Murman, E. M.: *Wind Tunnel Wall Interference Corrections for Aircraft Models in the Transonic Regime.* J. Airc., vol. 21 Jan. 1984, pp. 54-61.
14. Kemp, W. B., Jr.: *Computer Simulation of a Wind Tunnel Test Section With Discrete Finite-Length Wall Slots.* NASA CR-3948, Apr. 1986.
15. Kemp, W. B., Jr.: *A Panel Method Procedure for Interference Assessment in Slotted-Wall Wind Tunnels.* AIAA Paper no. 88-2537, June, 1988.
16. Thomas, J. L.; Luckring, J. M.; and Sellers, W. L., III: *Evaluation of Factors Determining the Accuracy of Linearized Subsonic Panel Methods.* AIAA Paper no. 83-1826, July, 1983.
17. Rust, Burt W.; and Burrus, Walter R.: *Mathematical Programming and the Numerical Solution of Linear Equations. Modern Analytical and Computational Methods in Science and Mathematics,* Richard Bellman, ed., American Elsevier Publishing Company, Inc., 1972, pp. 22-29.

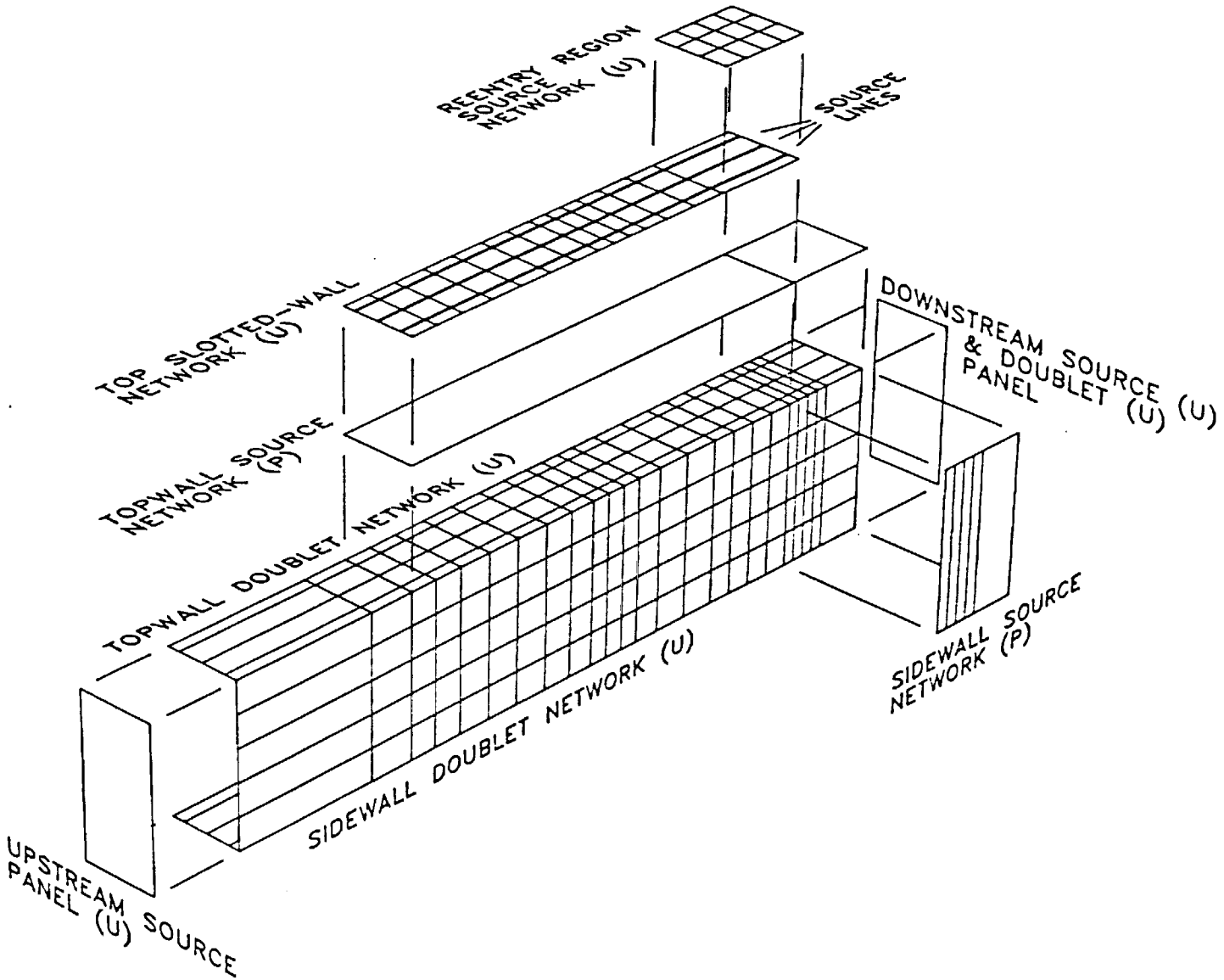

Figure 1. Panel networks used on boundary of tunnel flow domain.

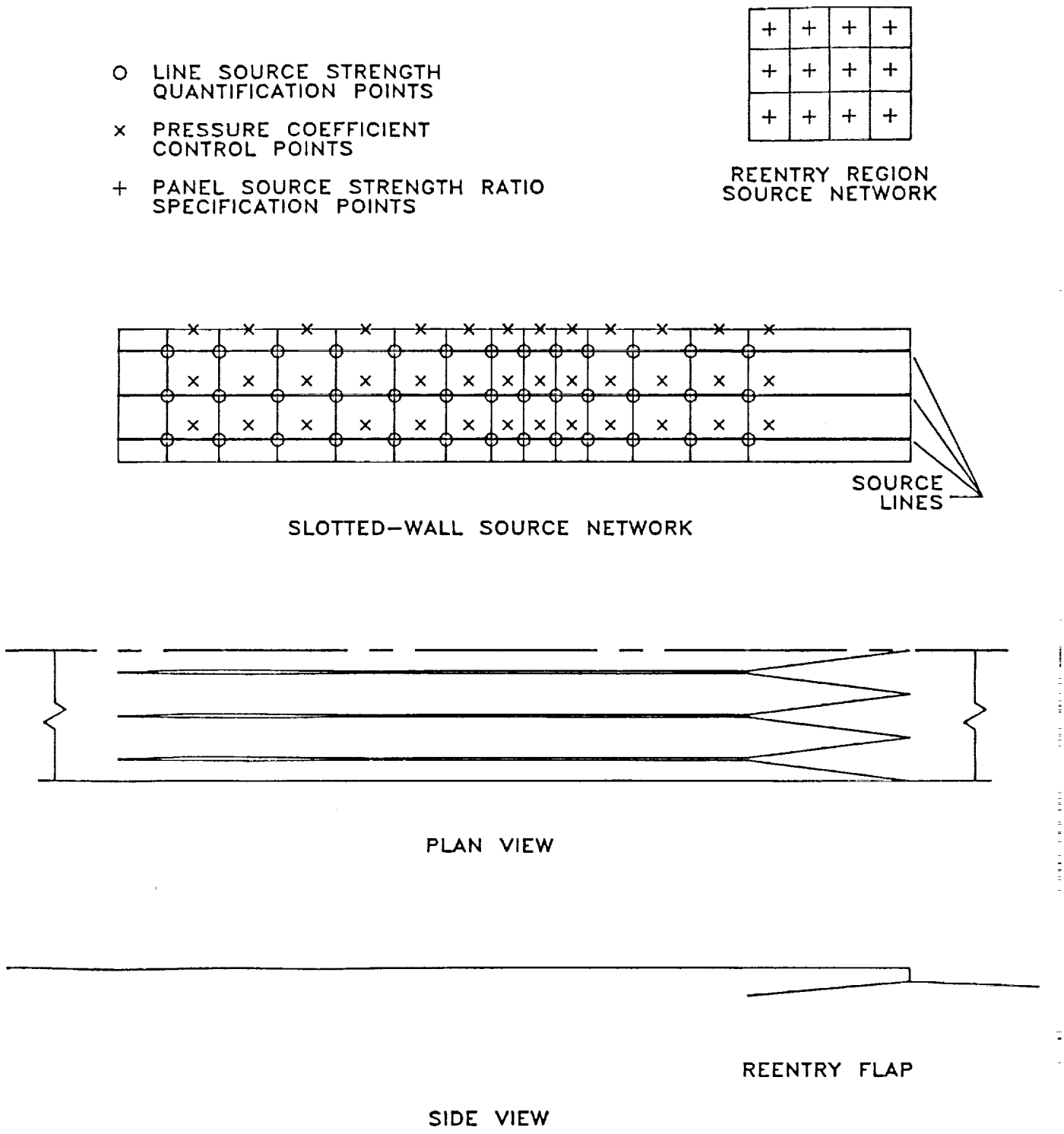

Figure 2. Special source panel networks for slotted-wall and reentry regions.

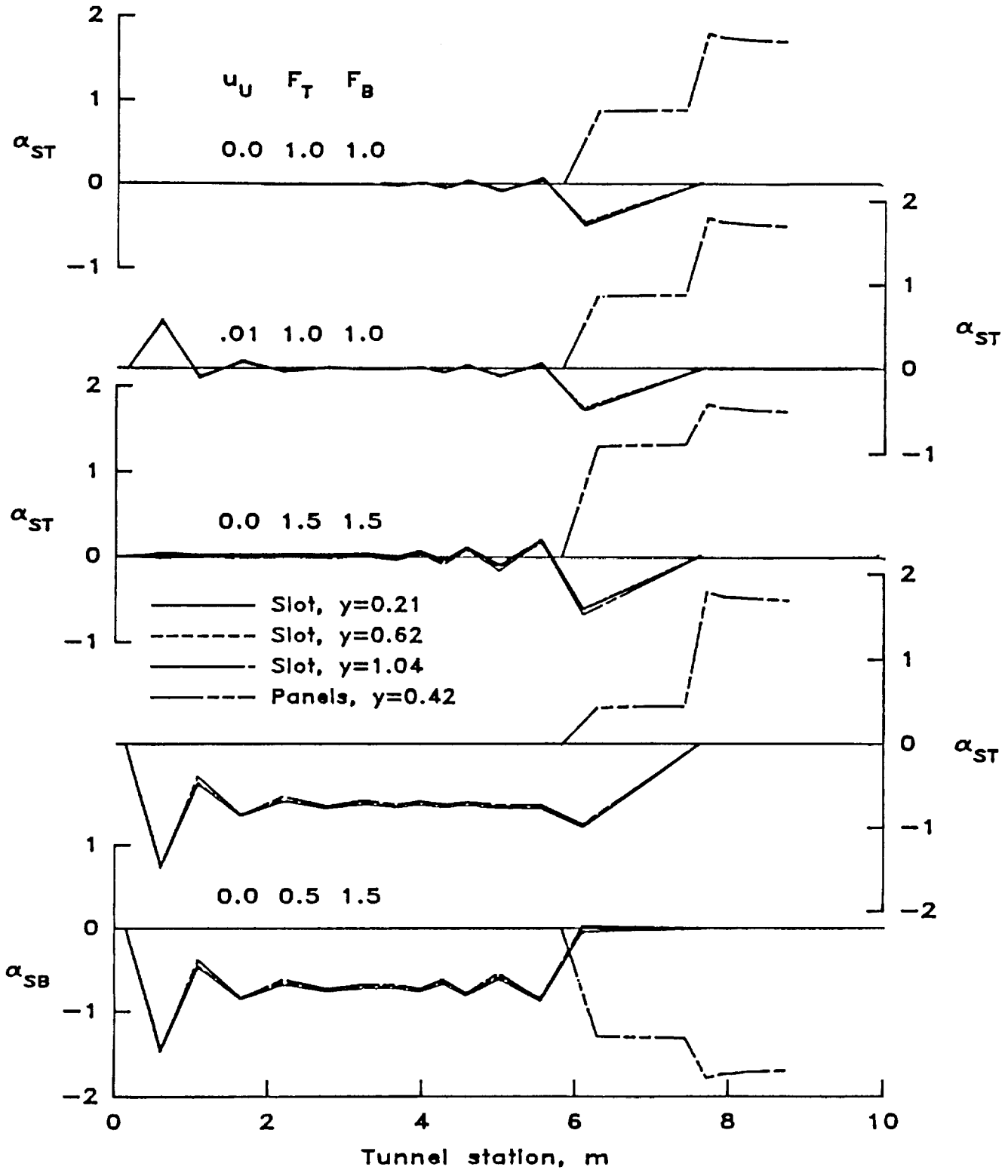

a. Flow angularity at wall slots and reentry region panels.

Figure 3. Effect of reentry region source panel strength on smoothness of slot flow.

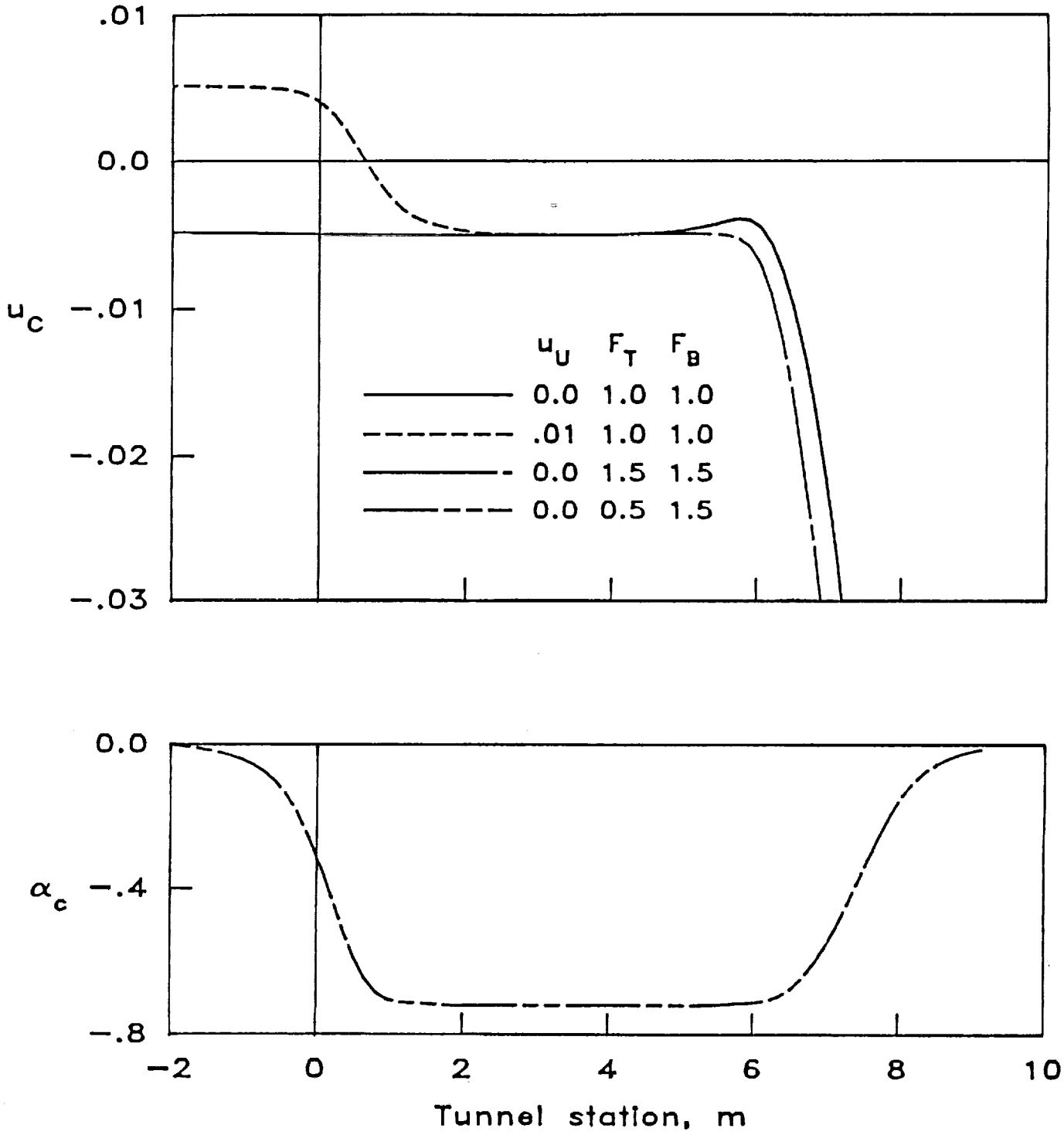

b. Flow perturbations on tunnel centerline.

Figure 3. Concluded.

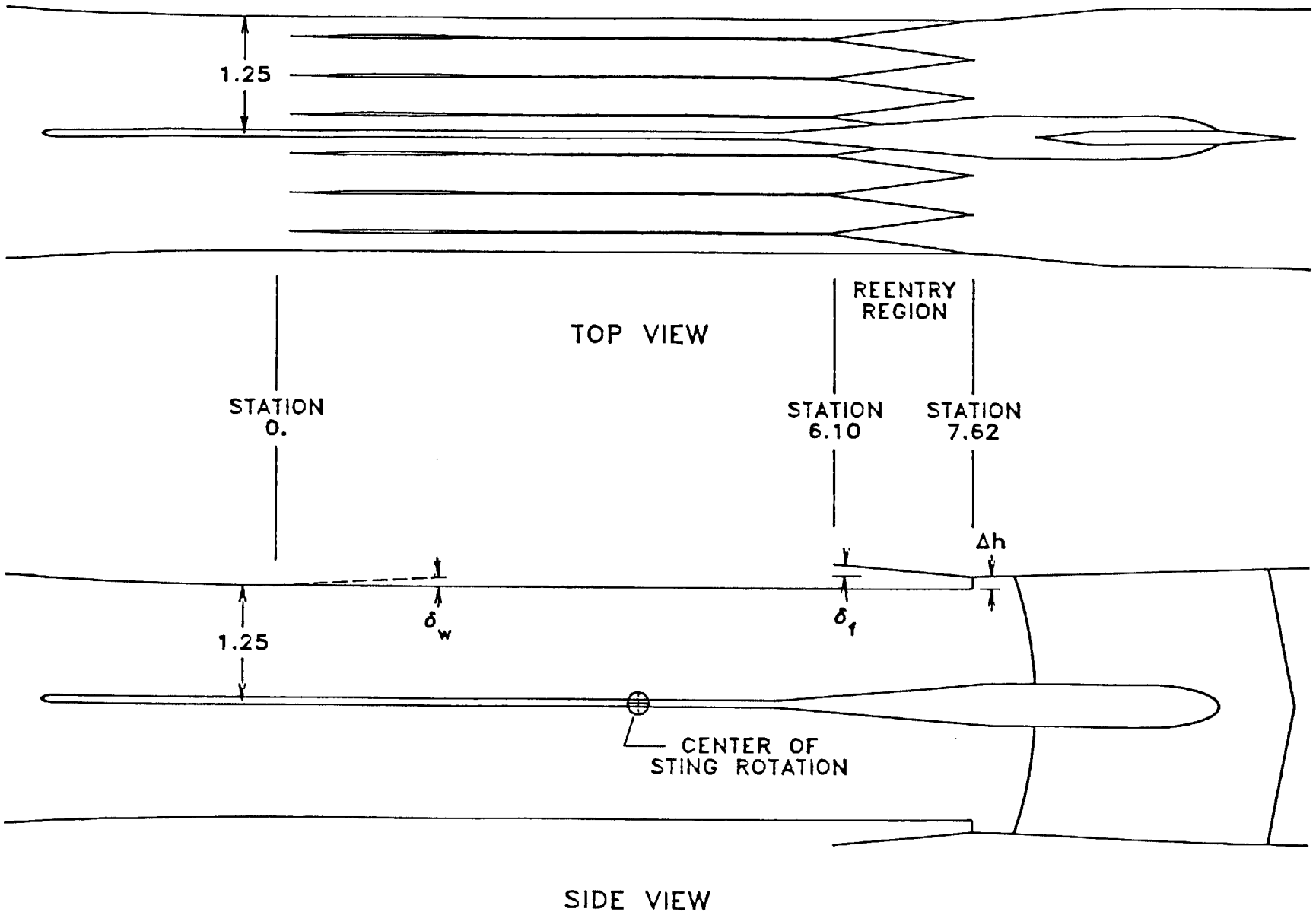

Figure 4. Sketch showing NTF test section geometry and centerline calibration probe installation. All dimensions in meters.

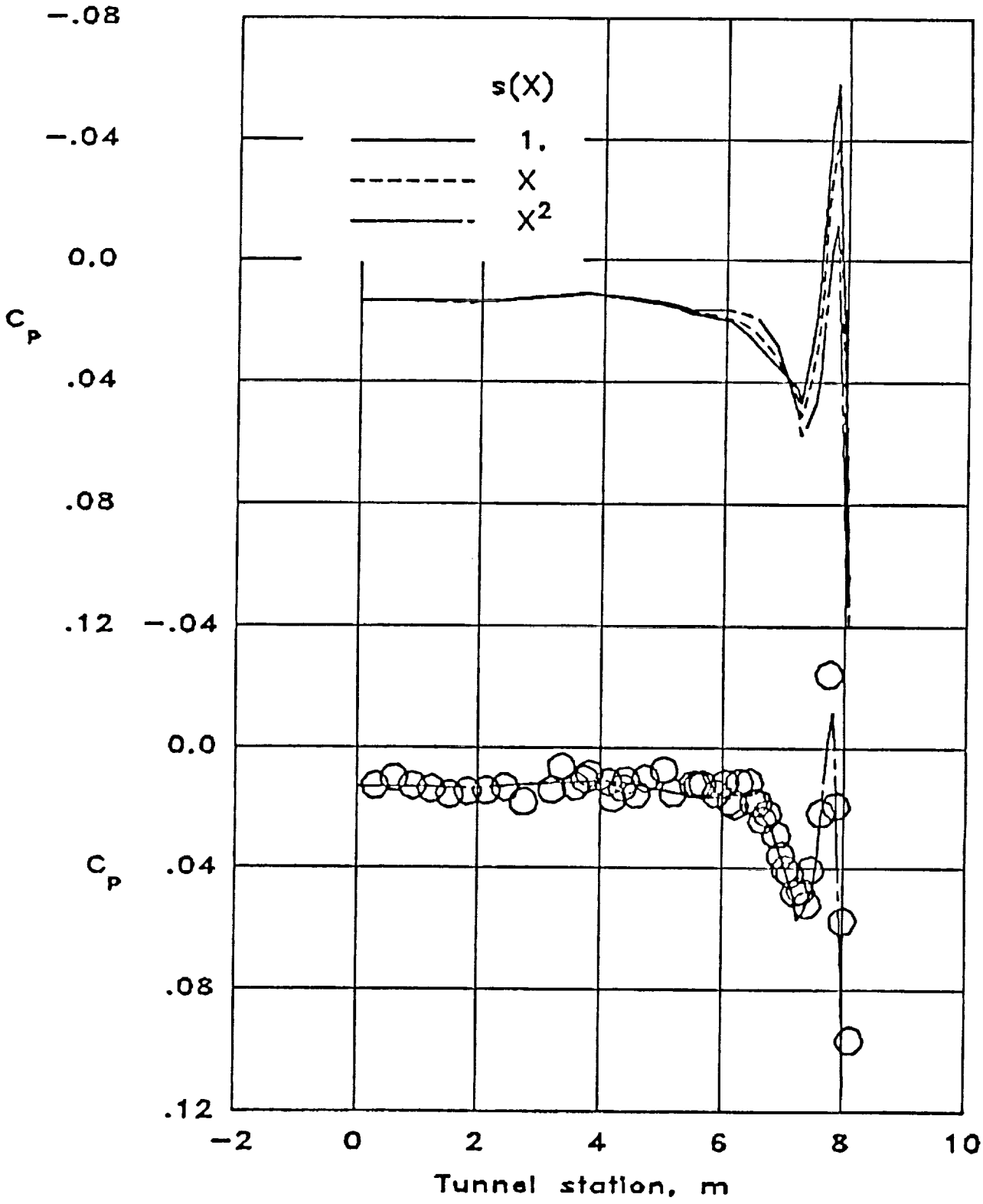

Figure 5. Effect of reentry region source shape function on pressure distribution on the sidewall center line and comparision with measured pressure distribution.

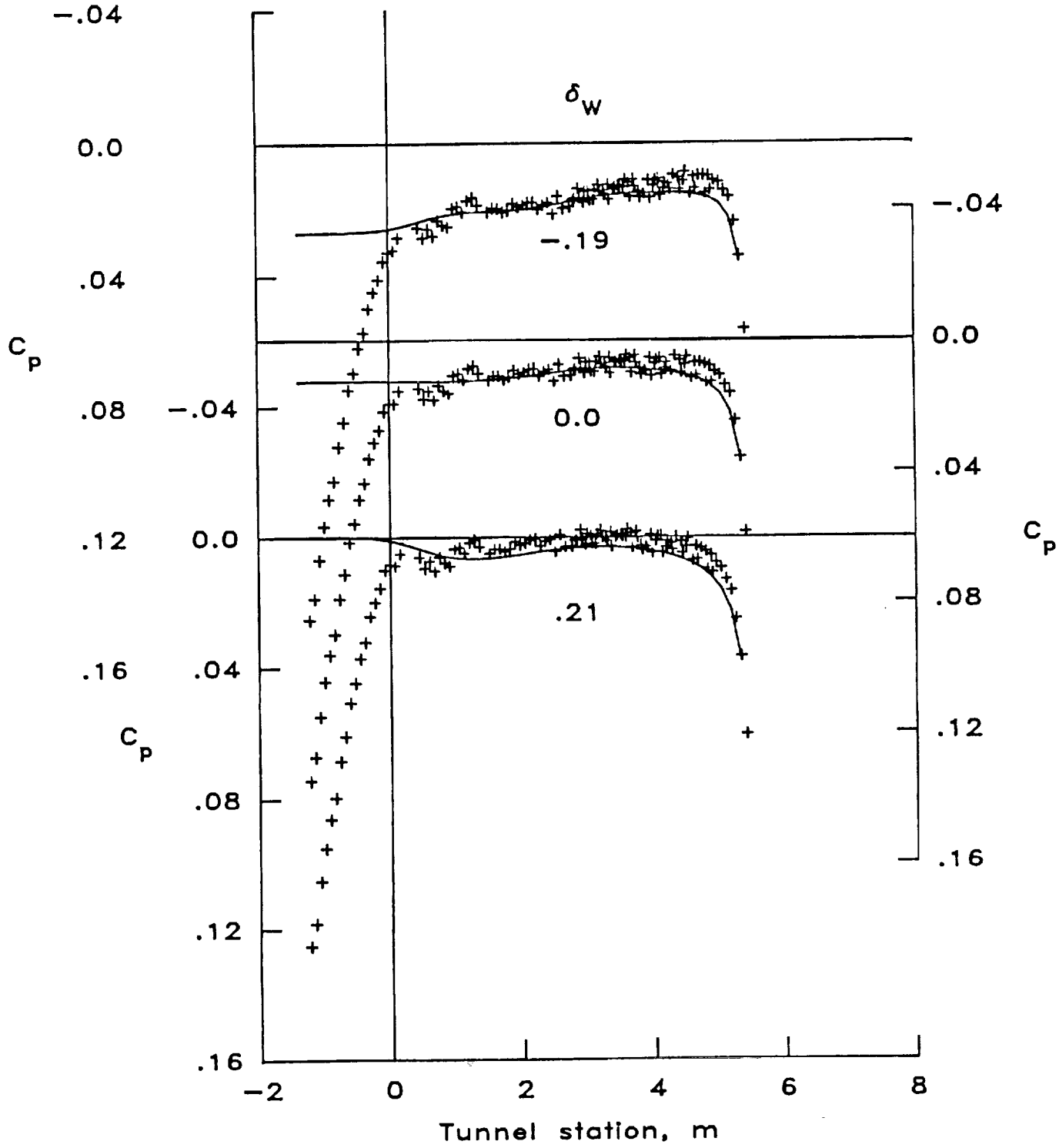

Figure 6. Comparison of calculated and measured pressure coefficients on surface of centerline calibration probe for three values of wall divergence setting. Symbols denote measured pressures. $R_u = 6.6 \times 10^6$.

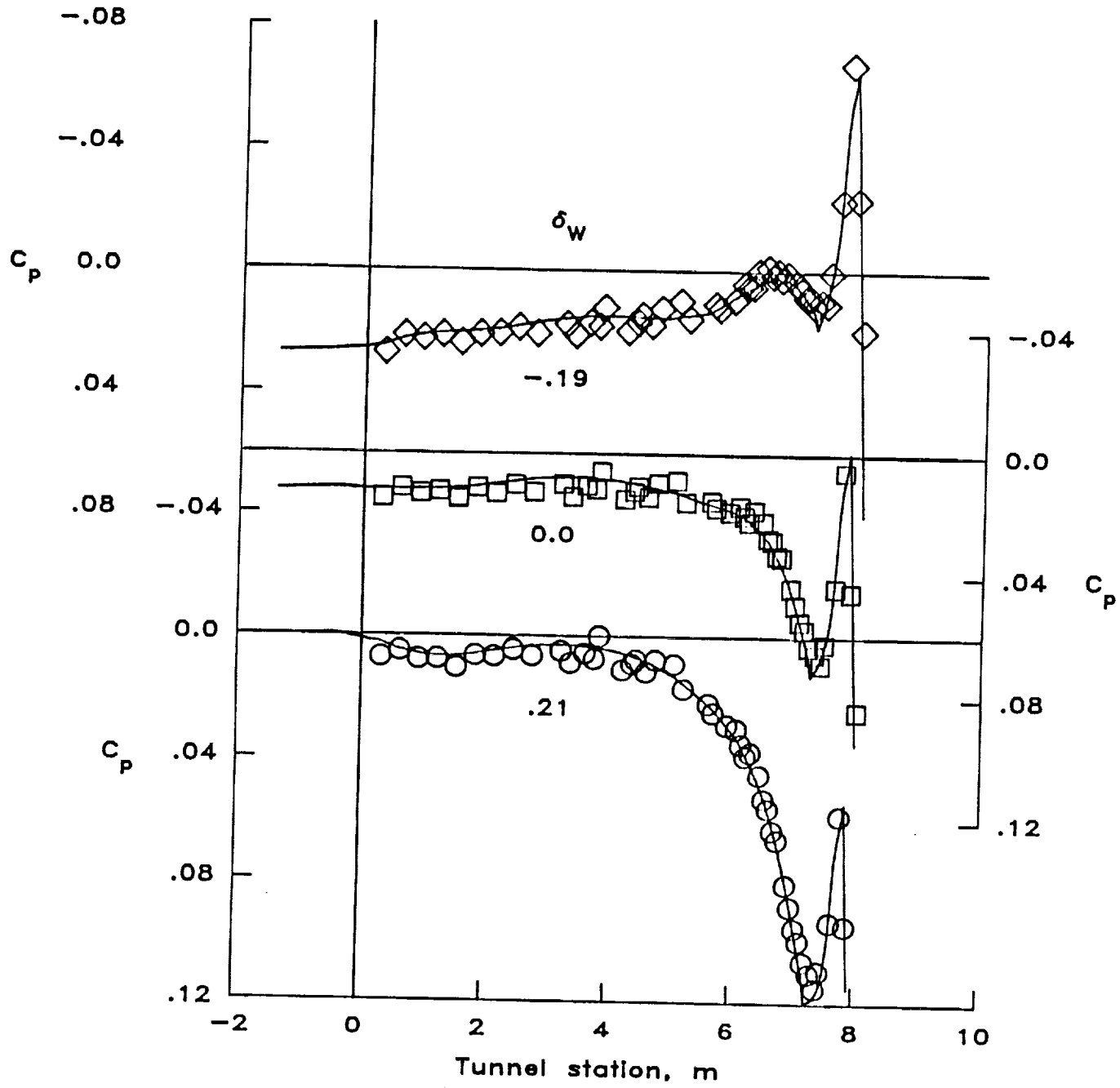

Figure 7. Comparison of calculated and measured pressure coefficients on the NTF sidewall center line for same test points as those of figure 6. Symbols denote measured pressures.

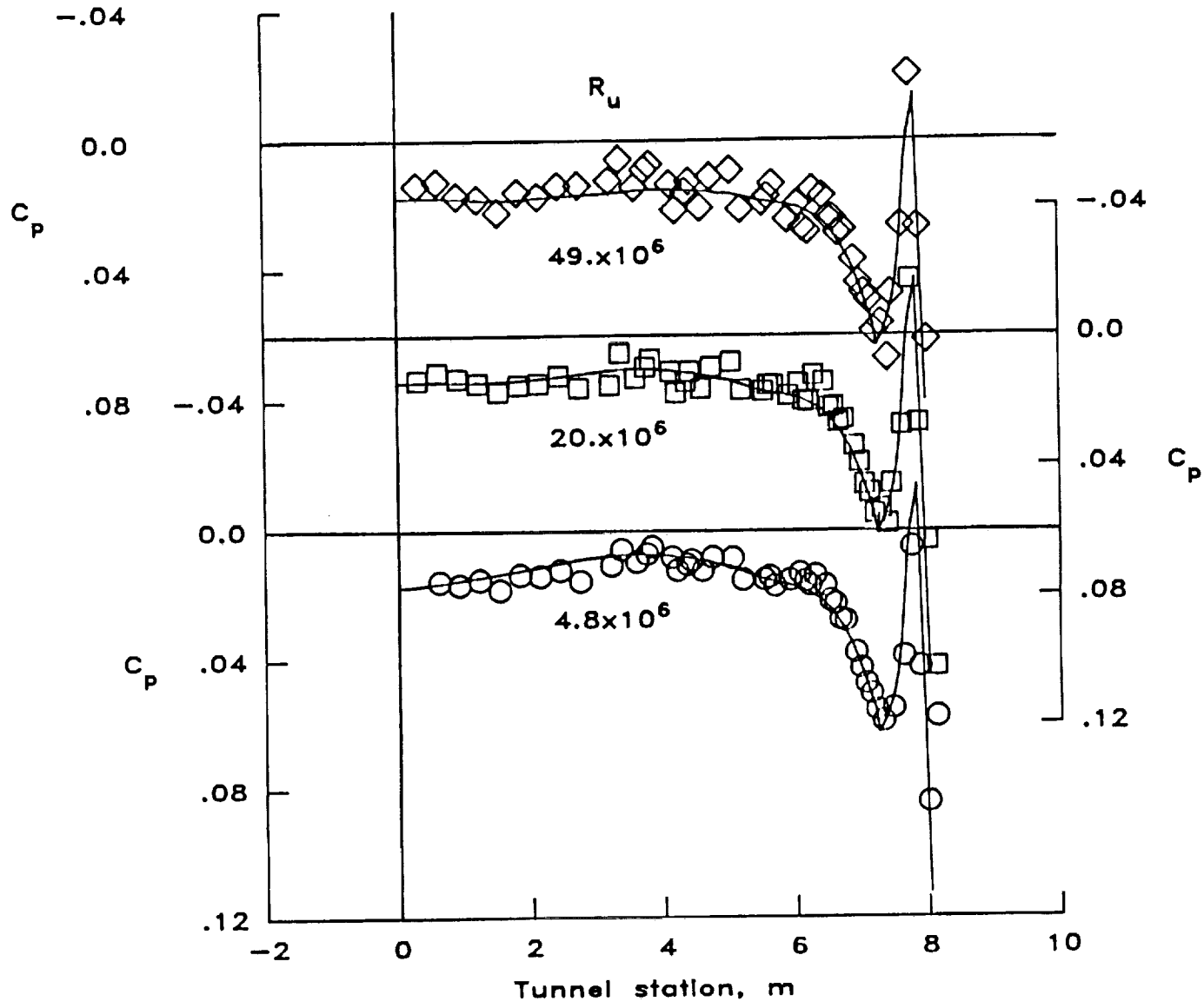

Figure 8. Comparison of calculated and measured pressure coefficients on the NTF sidewall center line for three values of unit Reynolds number. Symbols denote measured pressures. $\delta_w = -0.04 \pm .01$ deg.

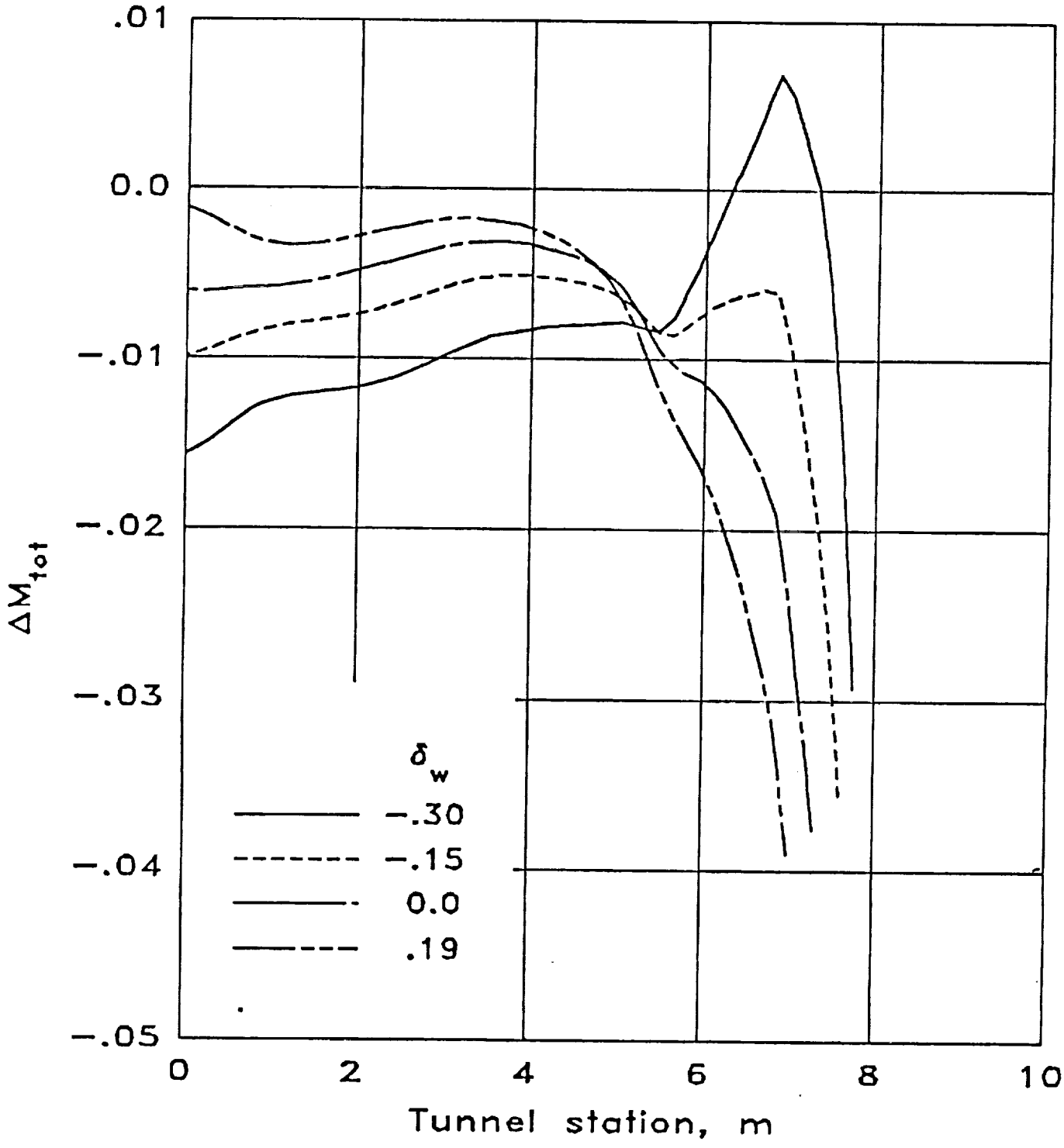

Figure 9. Effect of wall divergence setting on the Mach number component of total interference distribution on a survey line at $y = 0.625$ m, $z = 0$. $R_u = 4.8 \times 10^6$.

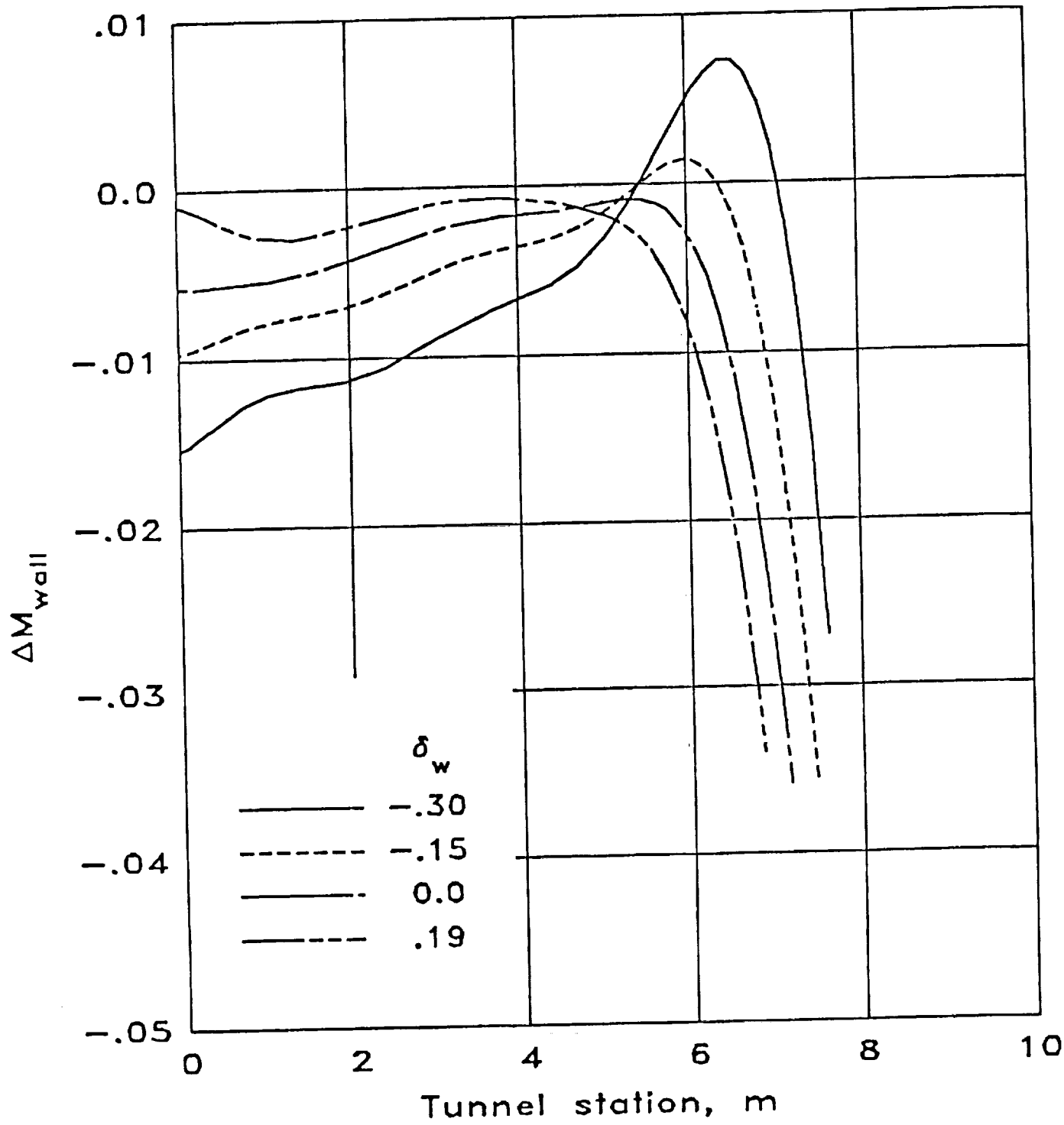

Figure 10. Effect of wall divergence setting on the Mach number component of wall interference for the same test conditions and survey location as those of figure 9.

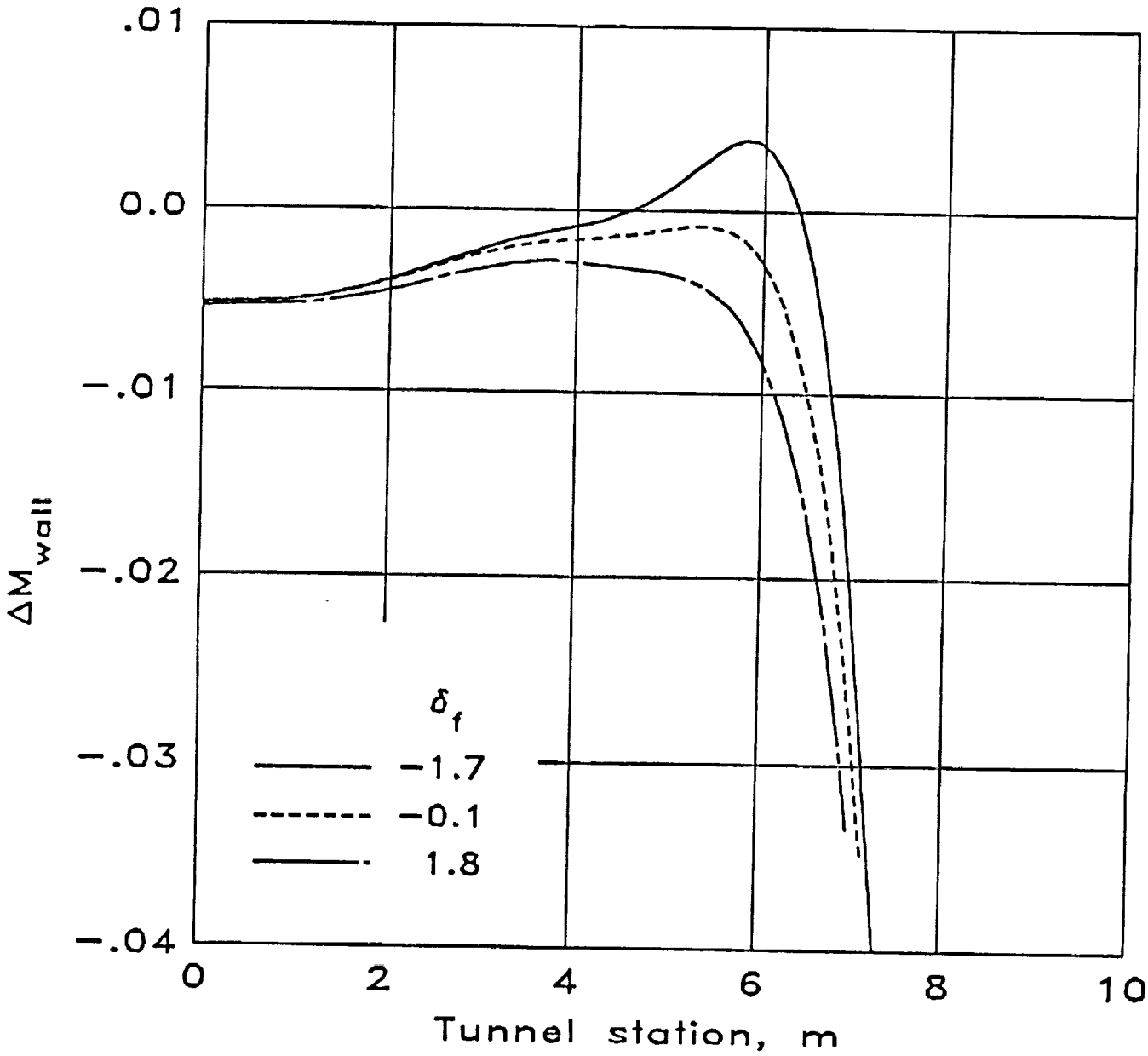

Figure 11. Effect of reentry flap setting on the Mach number component of wall interference distribution on a survey line at $y = 0.625$ m, $z = 0$. $R_u = 4.8 \times 10^6$.

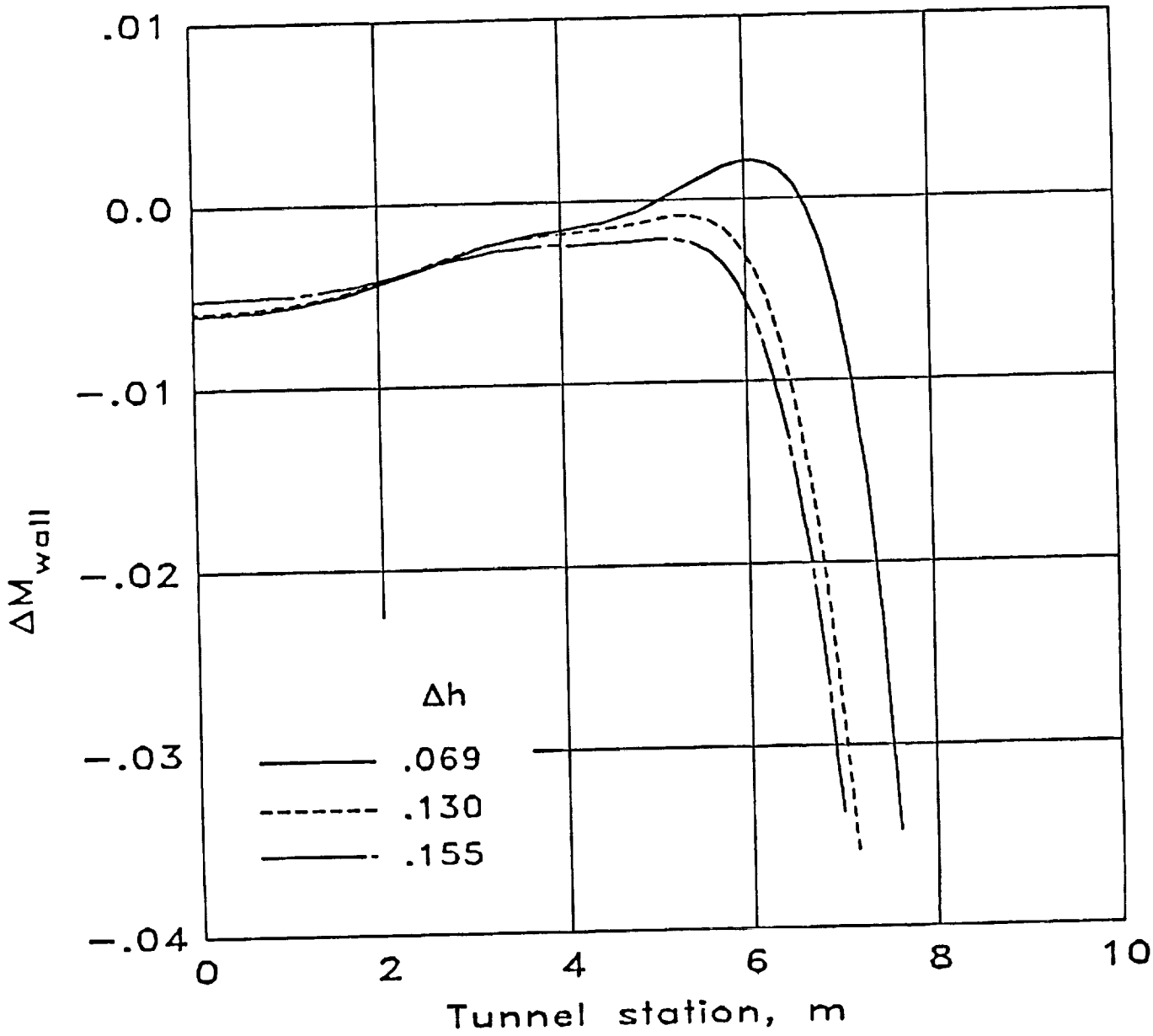

Figure 12. Effect of reentry step height on the Mach number component of wall interference distribution on a survey line at $y = 0.625$ m, $z = 0$. $R_u = 4.8 \times 10^6$.

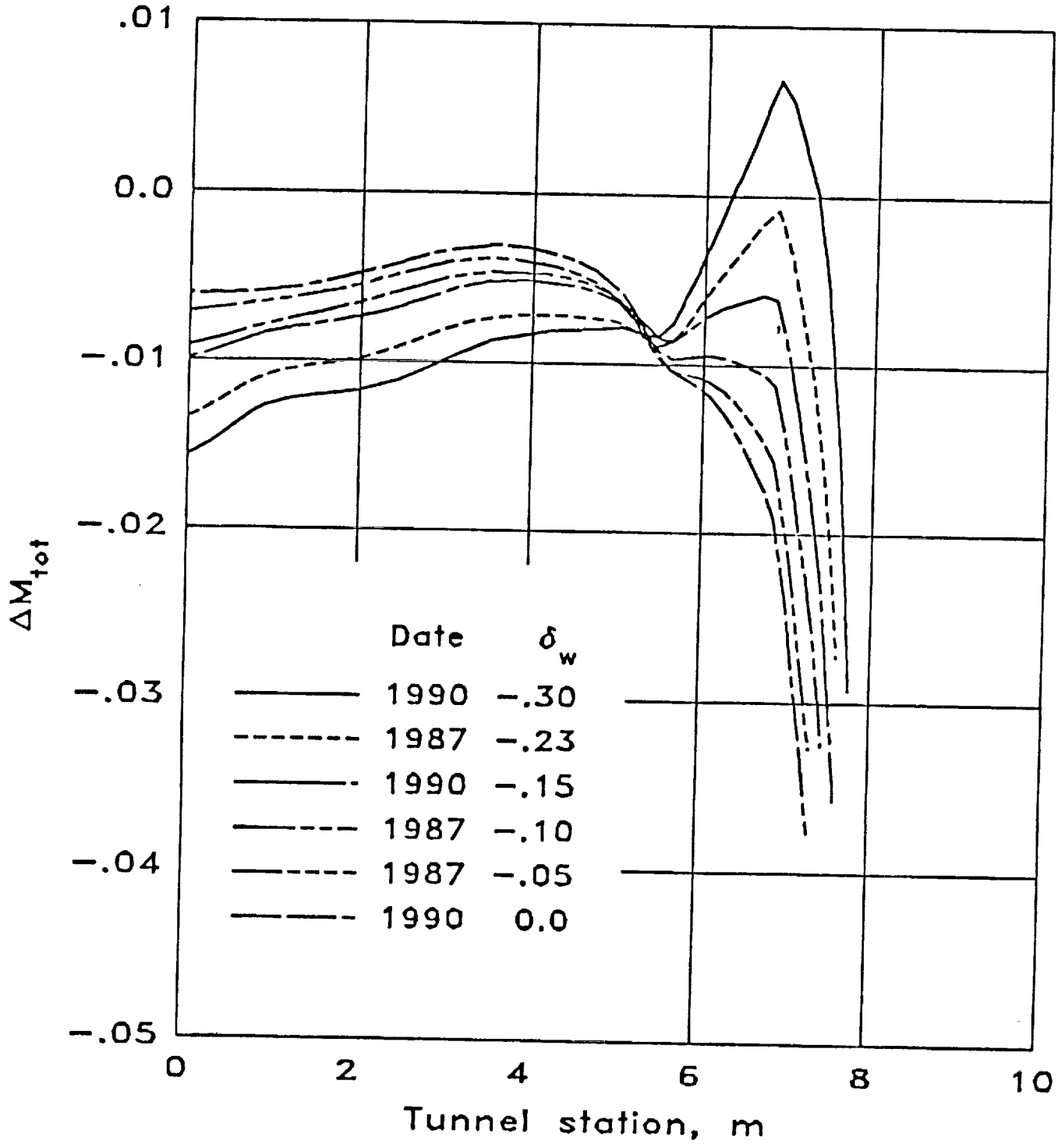

a. Mach number component of total interference.

Figure 13. Comparison of assessed interference results from NTF calibration tests in 1987 and 1990. Survey line at $y = 0.625$ m, $z = 0$. $R_u = 4.8 \times 10^6$.

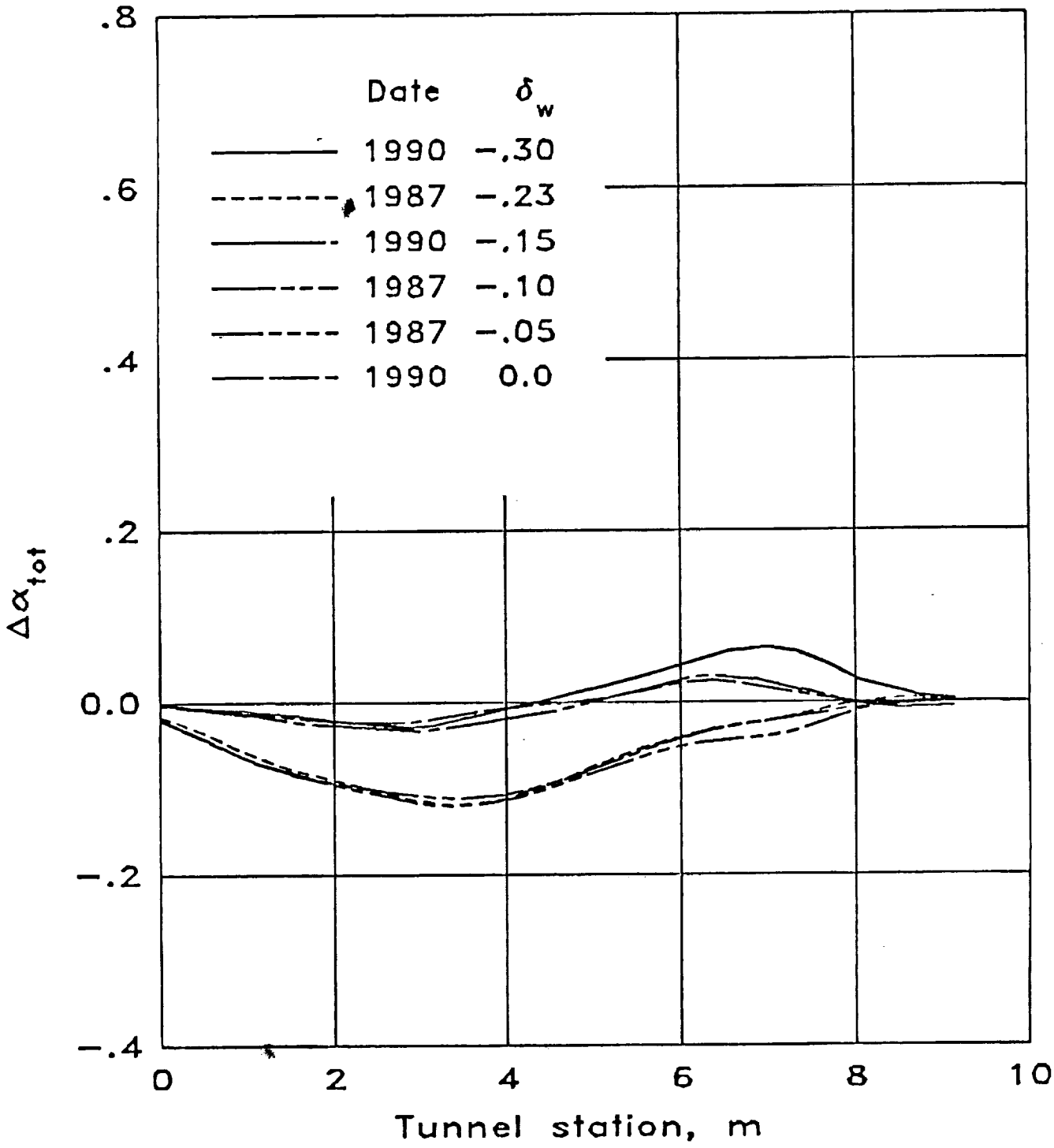

b. Flow angle component of total interference.

Figure 13. Concluded.

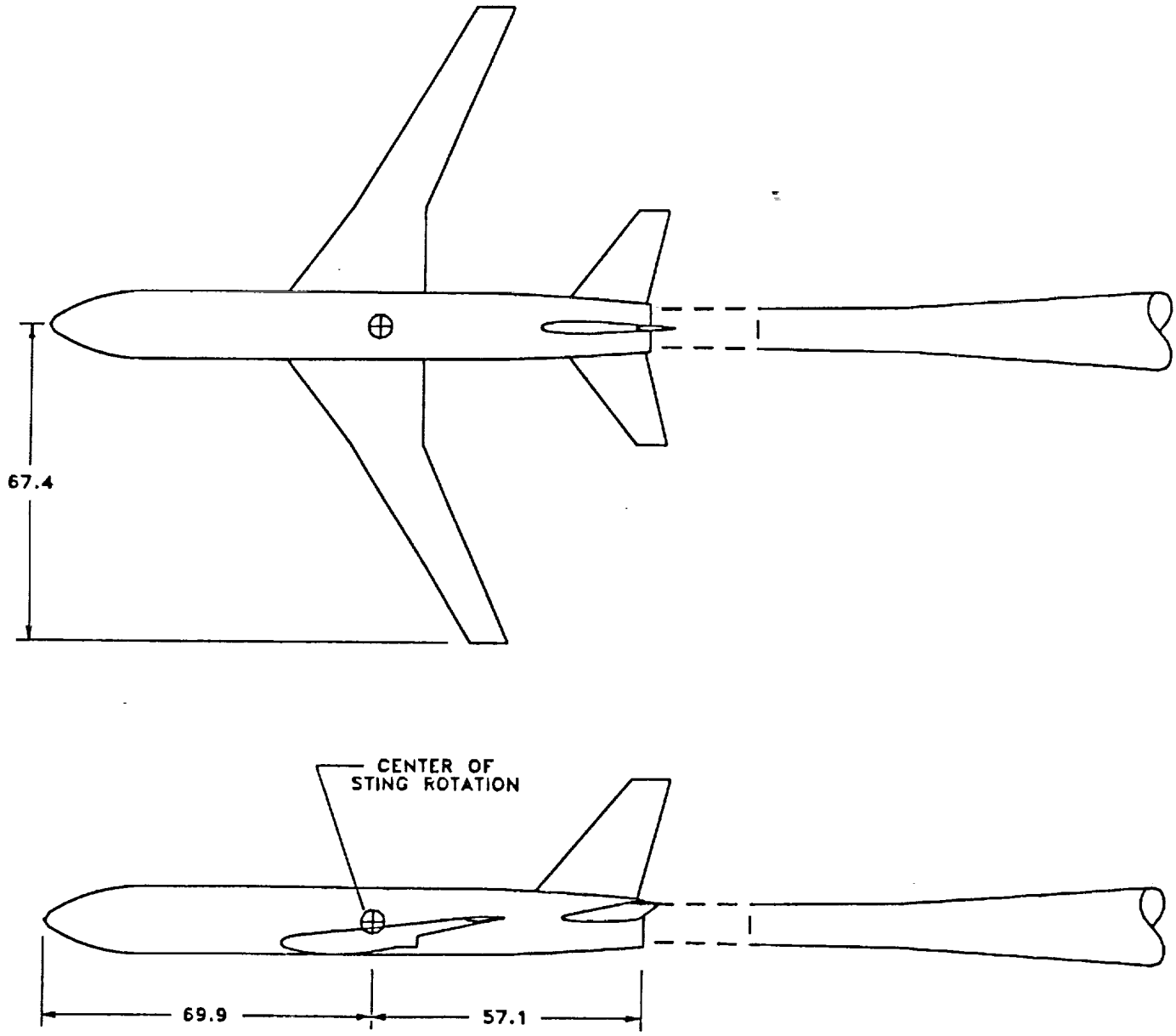

Figure 14. Sketch of the Pathfinder I model and part of its support sting. All dimensions in cm.

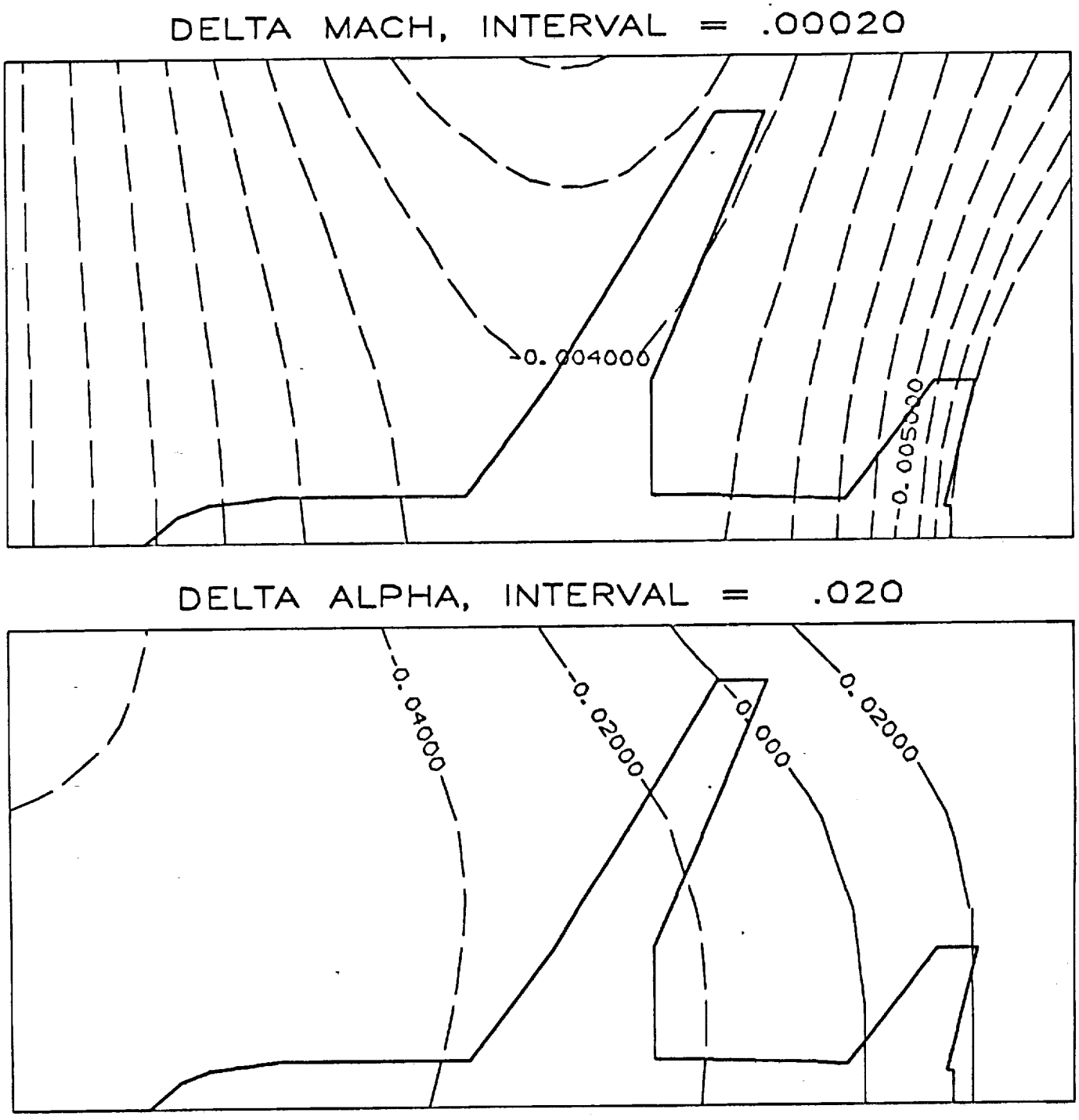

Figure 15. Contour plots of assessed total interference components for a typical test point of the Pathfinder I tests. $C_L = 0.514$, $R_u = 3.2 \times 10^6$, $\delta_w = -0.11$ deg.

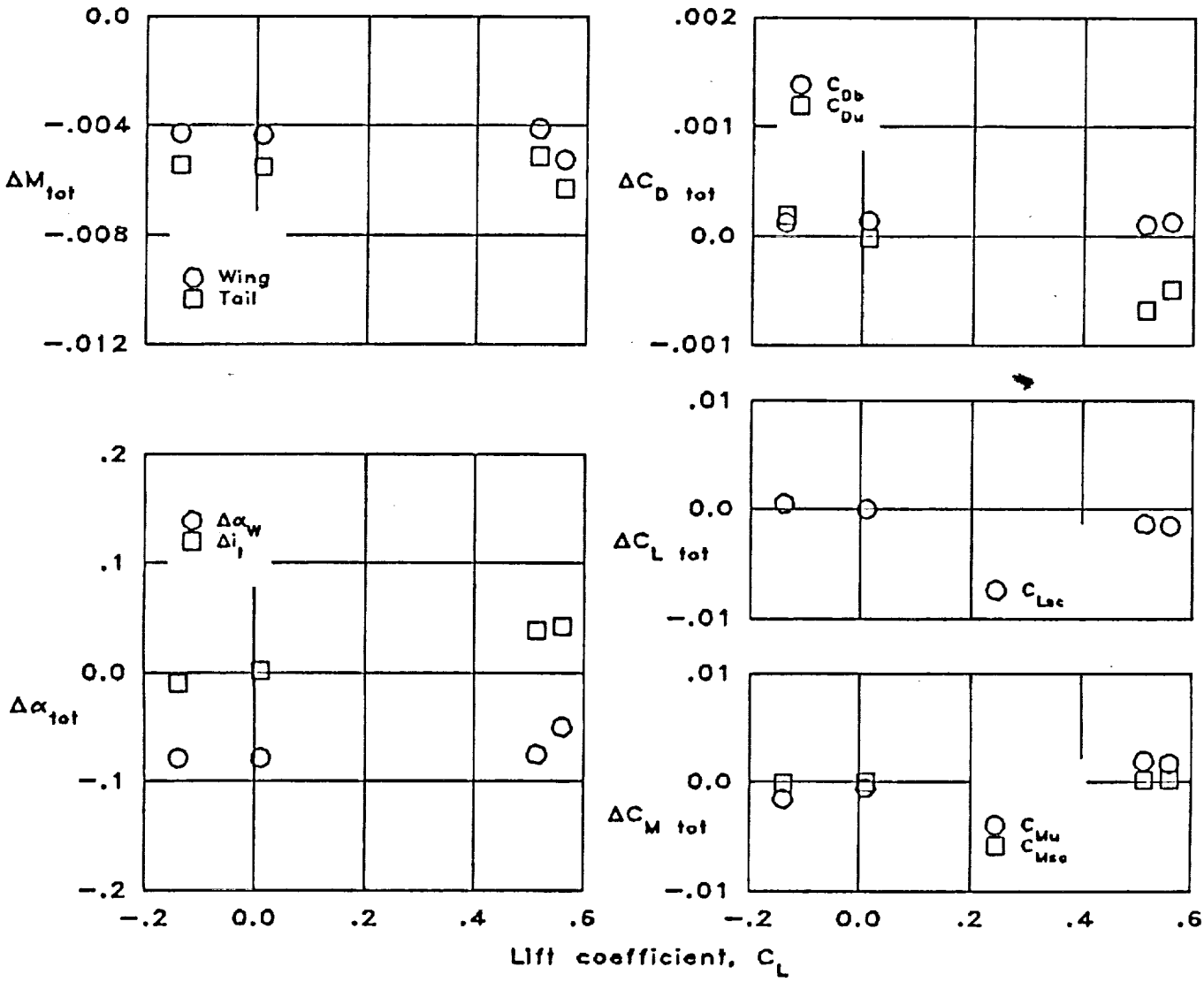

Figure 16. Assessed total interference corrections to model data for a typical test run of the Pathfinder I tests. $R_u = 3.2 \times 10^6$, $\delta_w = -0.11$ deg.

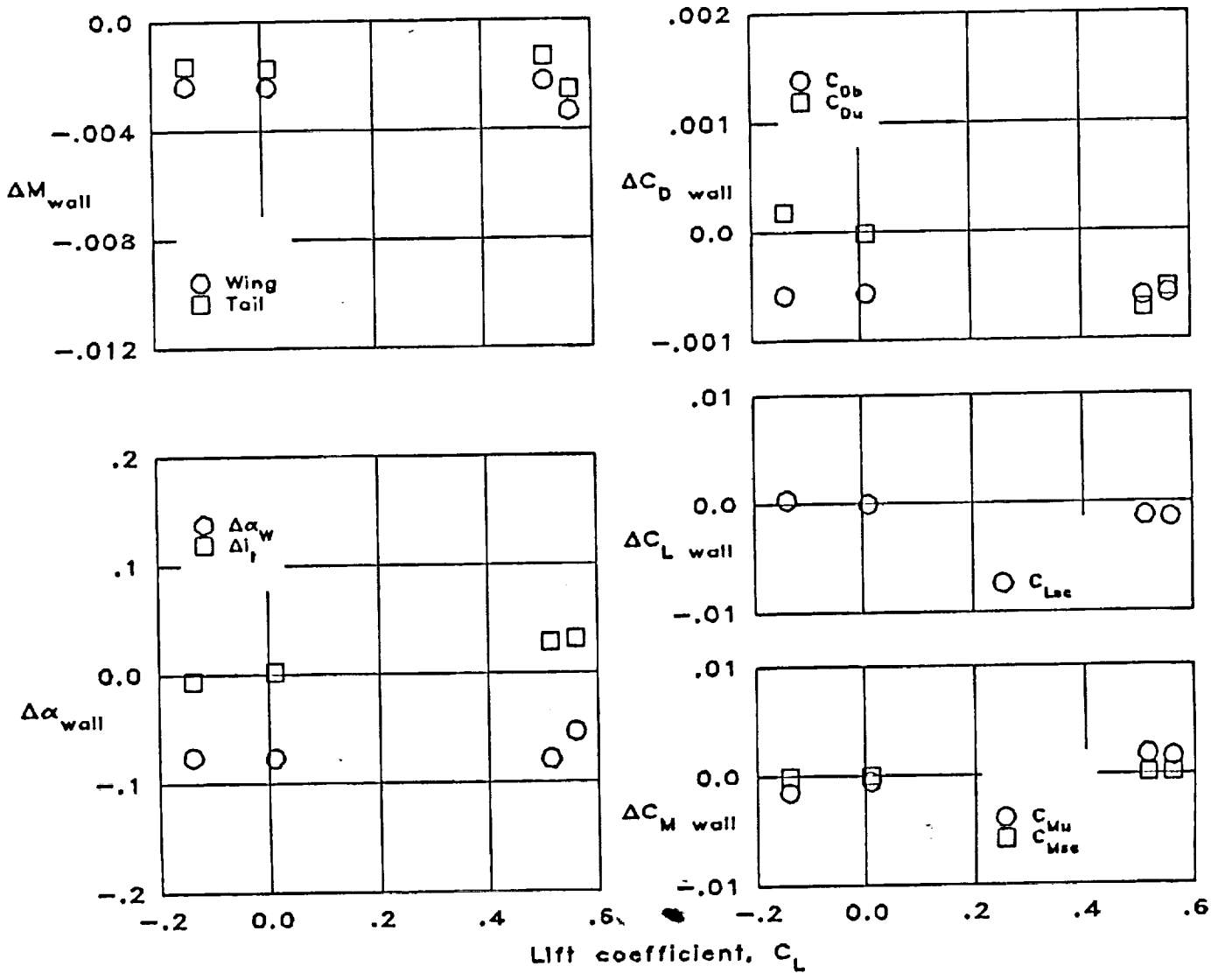

Figure 17. Assessed wall interference corrections (direct contribution of sting omitted) to model data for the same Pathfinder I test run as that of figure 16.

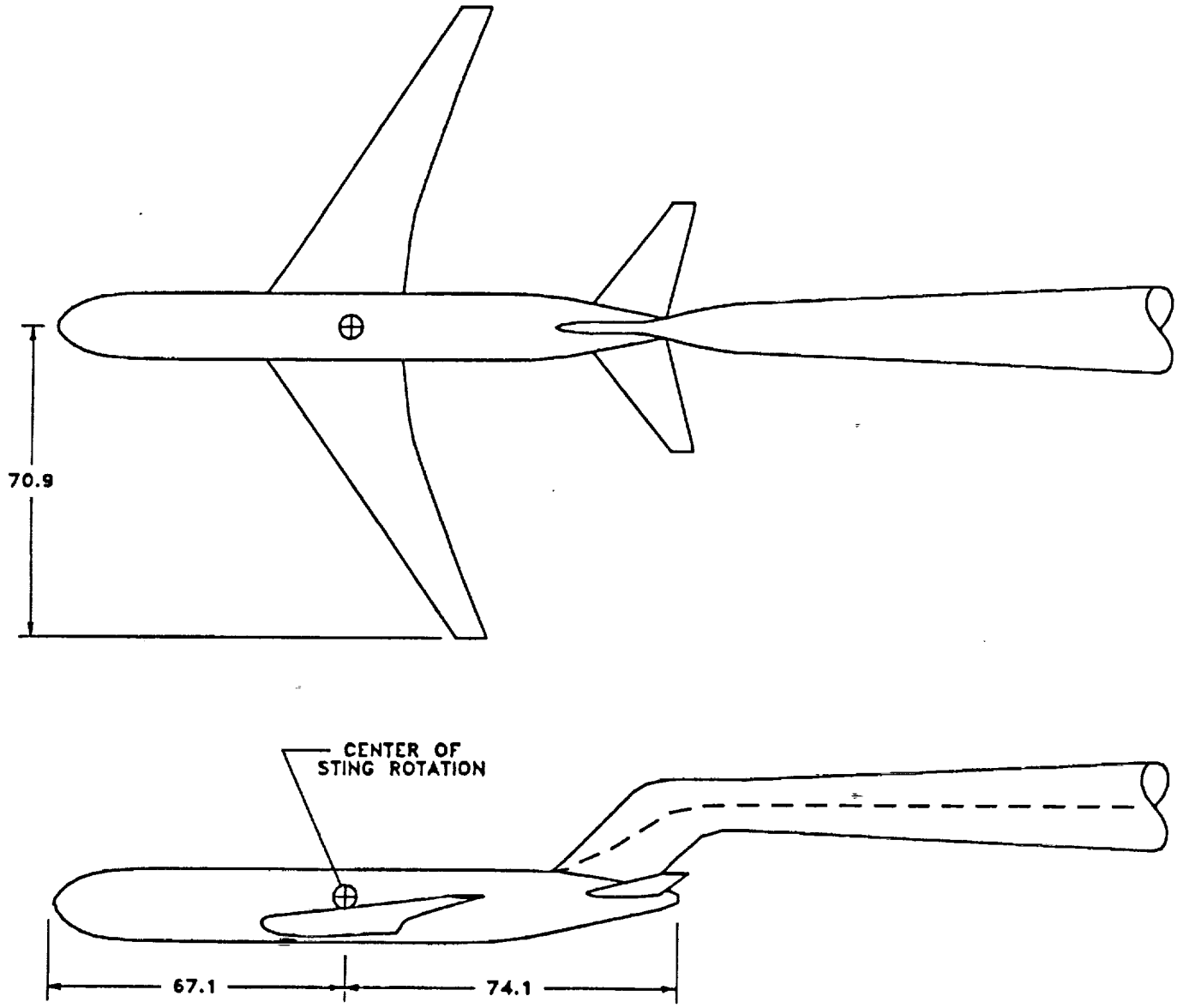

Figure 18. Sketch of the Boeing 767 model and part of its swept-strut model support system. Nacelles and pylons are omitted from the sketch. All dimensions in cm.

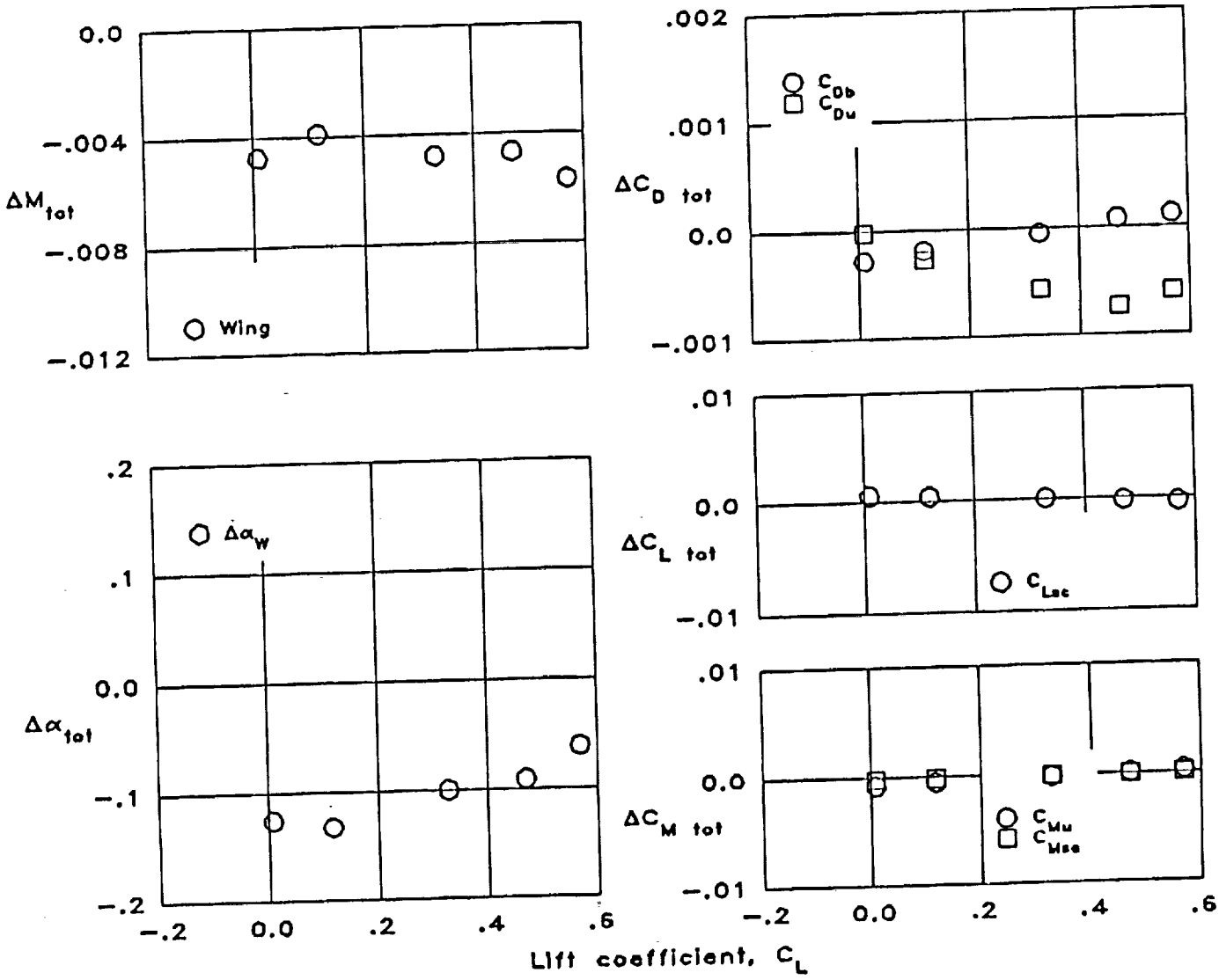

Figure 19. Assessed total interference corrections to model data for the B767 model with horizontal tail removed. $R_u = 6.1 \times 10^6$, $\delta_w = -0.11$ deg.

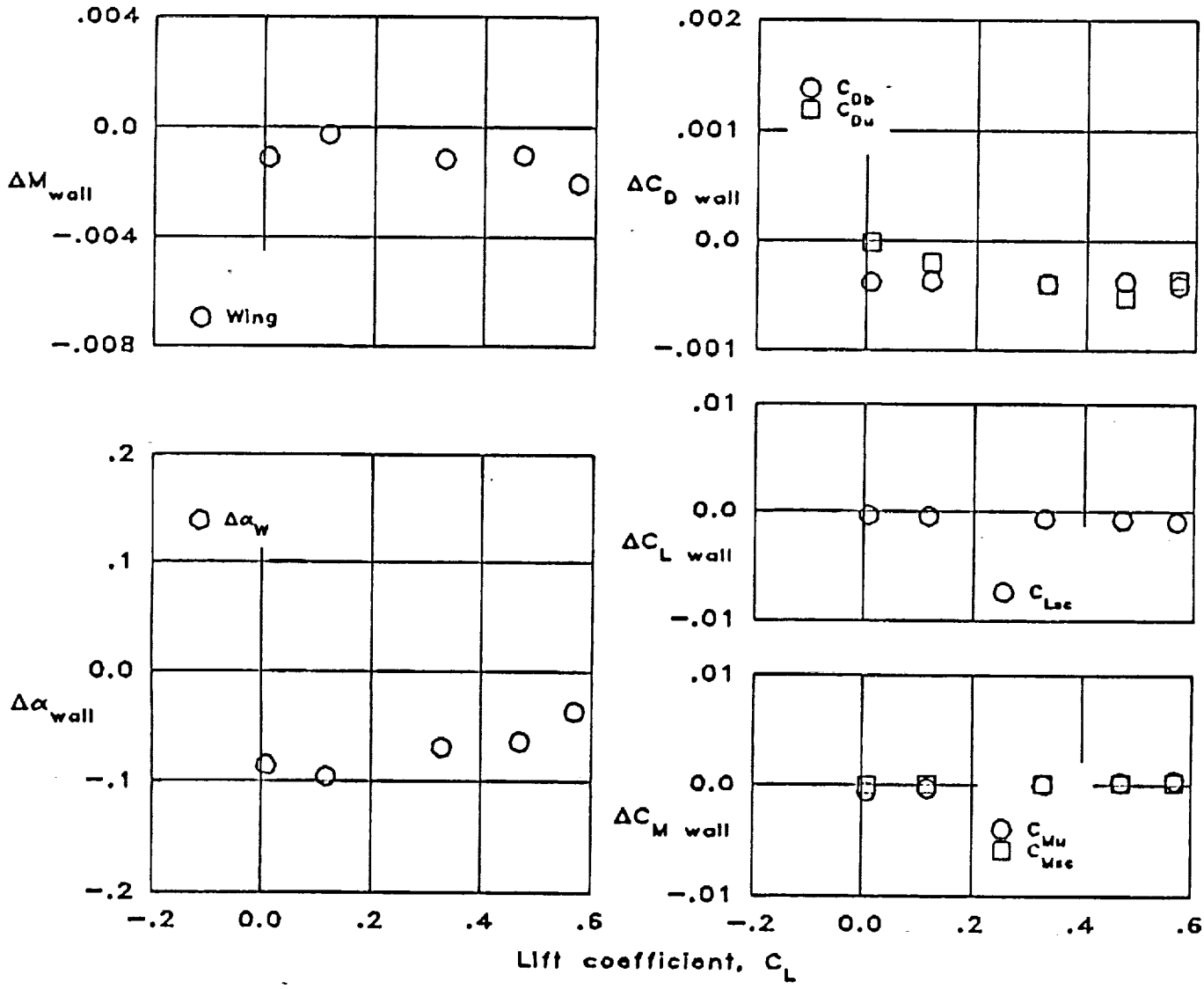

Figure 20. Assessed wall interference corrections to model data for the same B767 test run as that of figure 19.

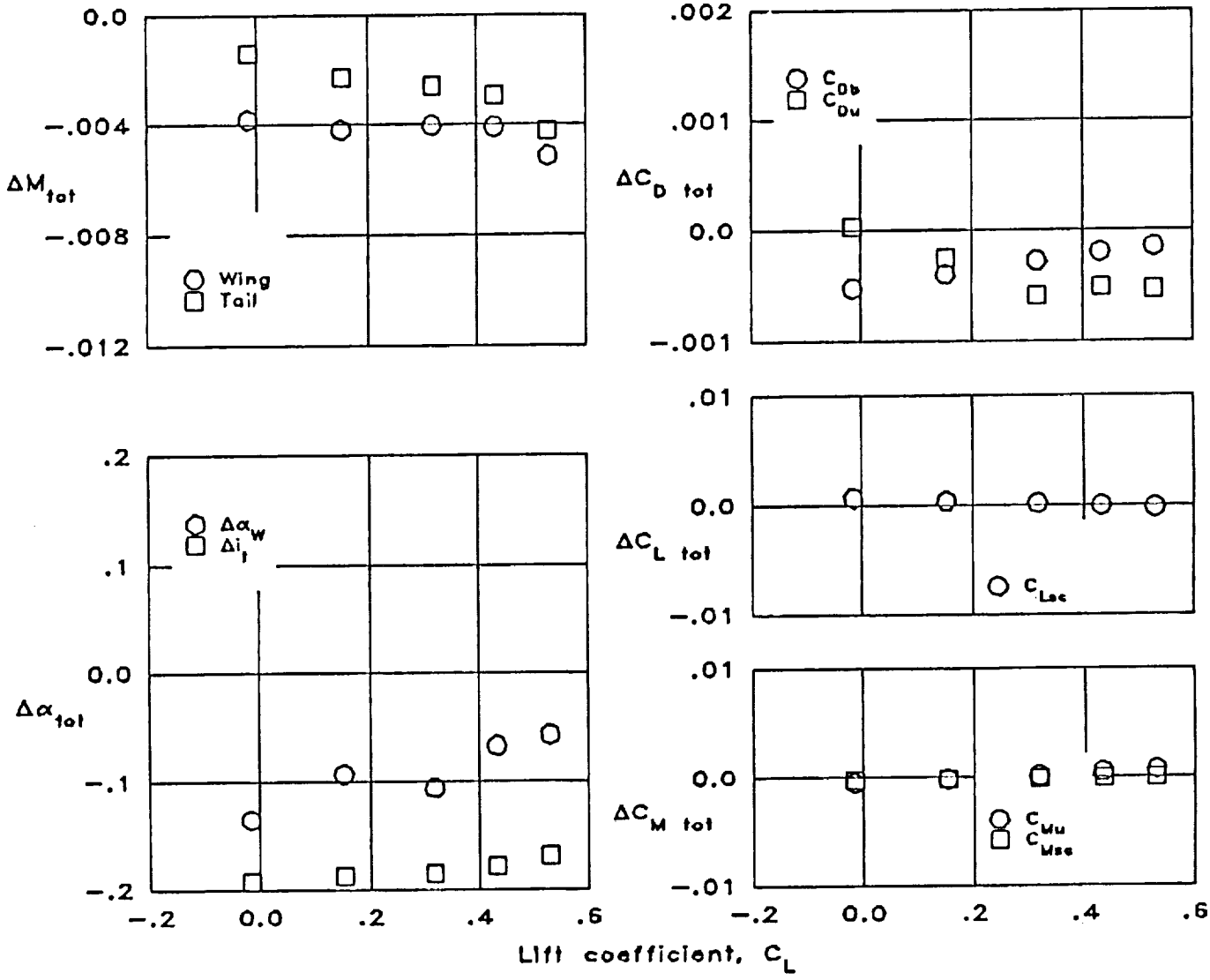

Figure 21. Assessed total interference corrections to model data for the complete B767 model. $R_u = 6.1 \times 10^6$, $\delta_w = -0.11$ deg.

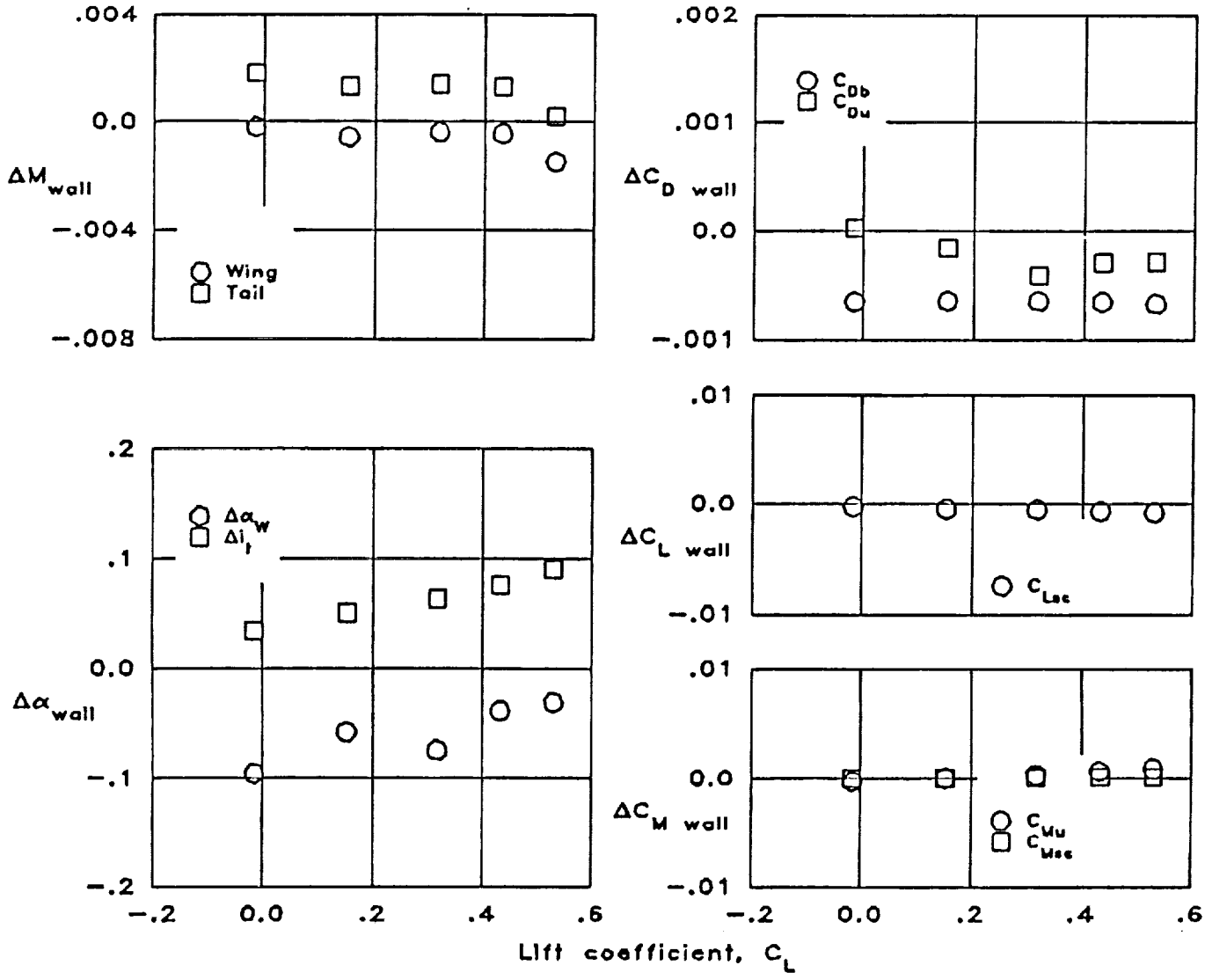

Figure 22. Assessed wall interference corrections to model data for the same B767 test run as that of figure 21.

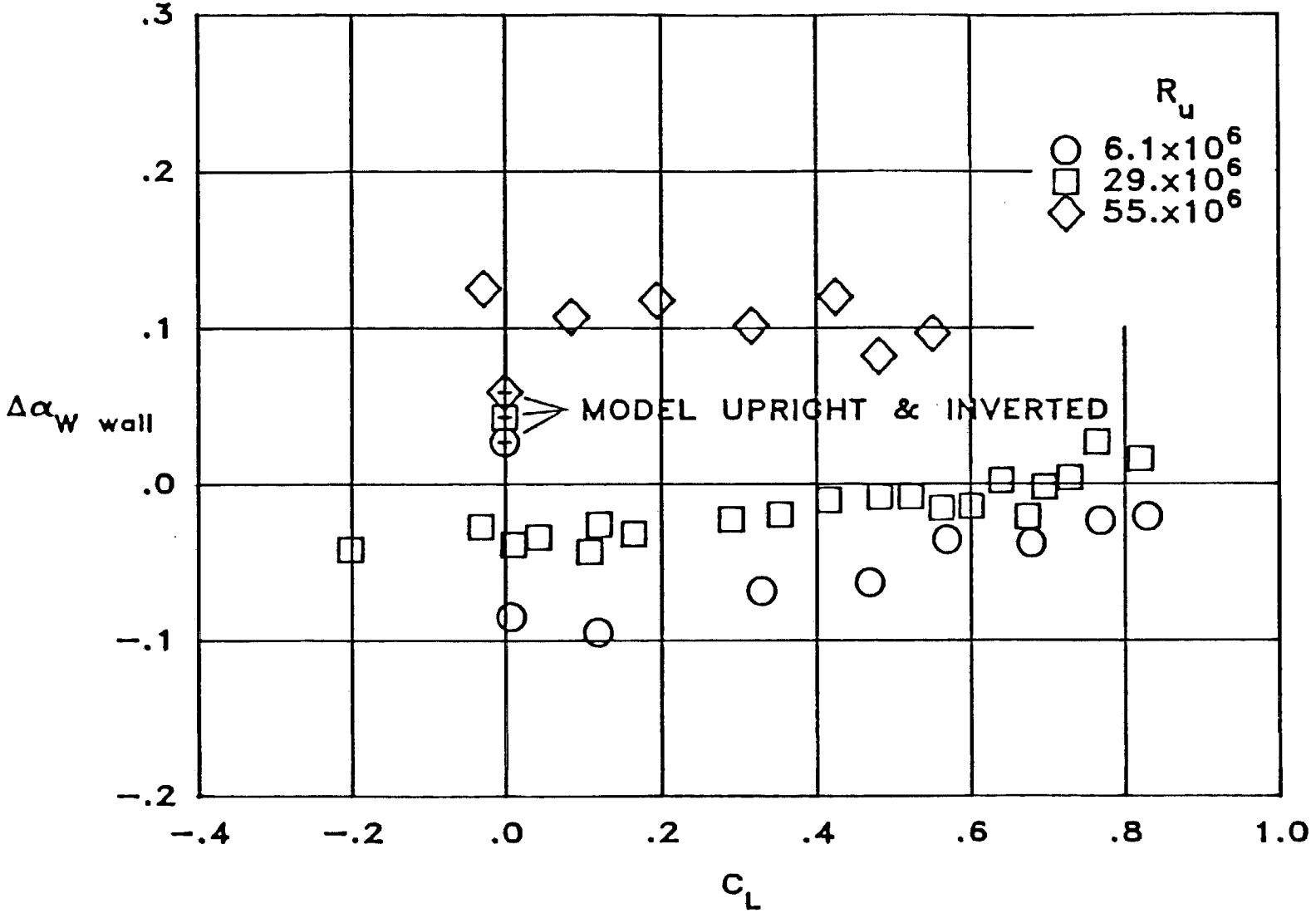

Figure 23. Effect of unit Reynolds number on the assessed flow angularity component of wall interference for the complete B767 model. Flow angles from model erect and inverted tests included for comparison. δ_w varies from -0.11 to +0.03 deg. depending on R_u.

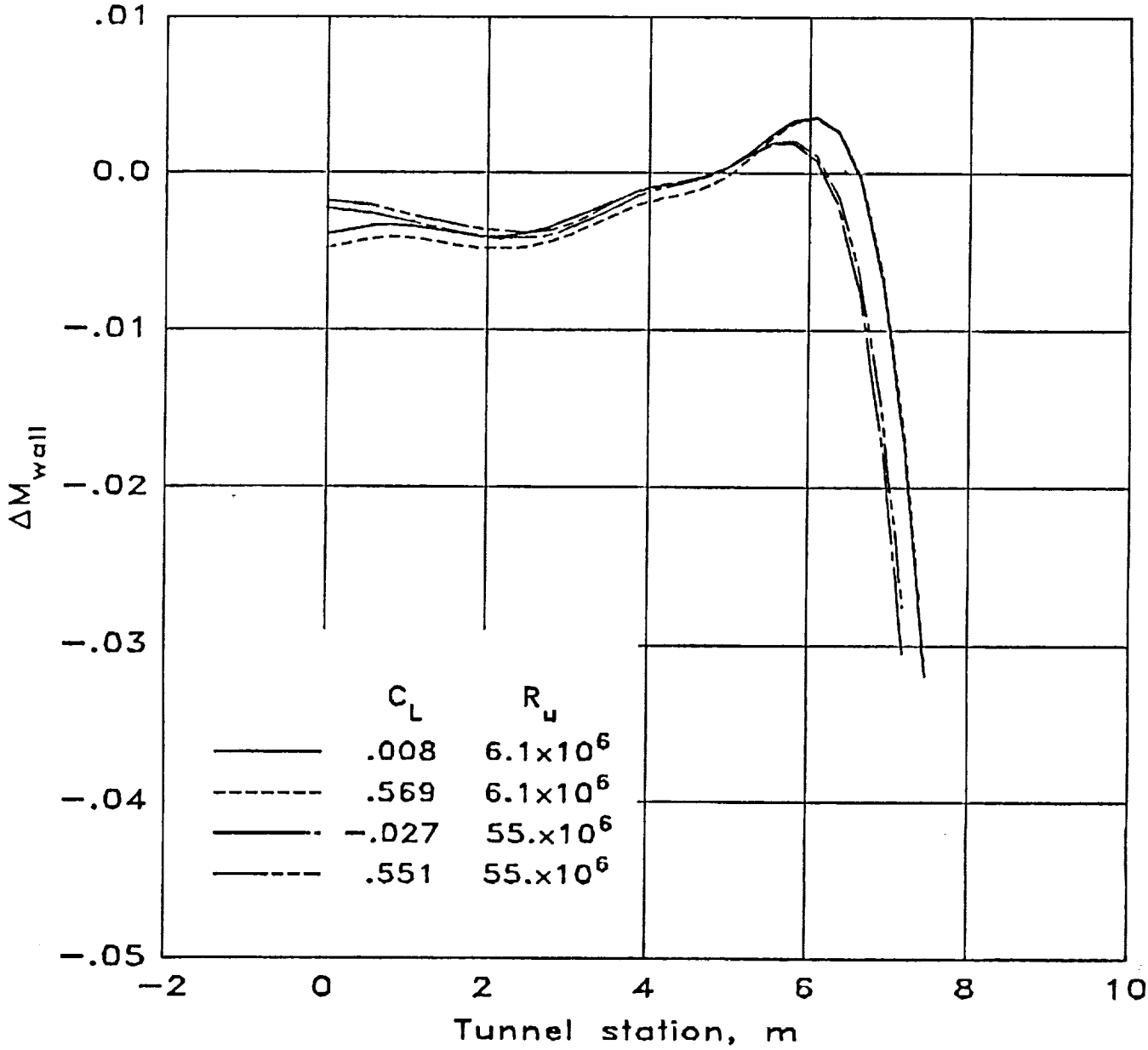

a. Mach number component of wall interference.

Figure 24. Effect of unit Reynolds number and B767 model lift coefficient on assessed wall interference distribution on a survey line at $y = 0.625$ m and $z = 0$.

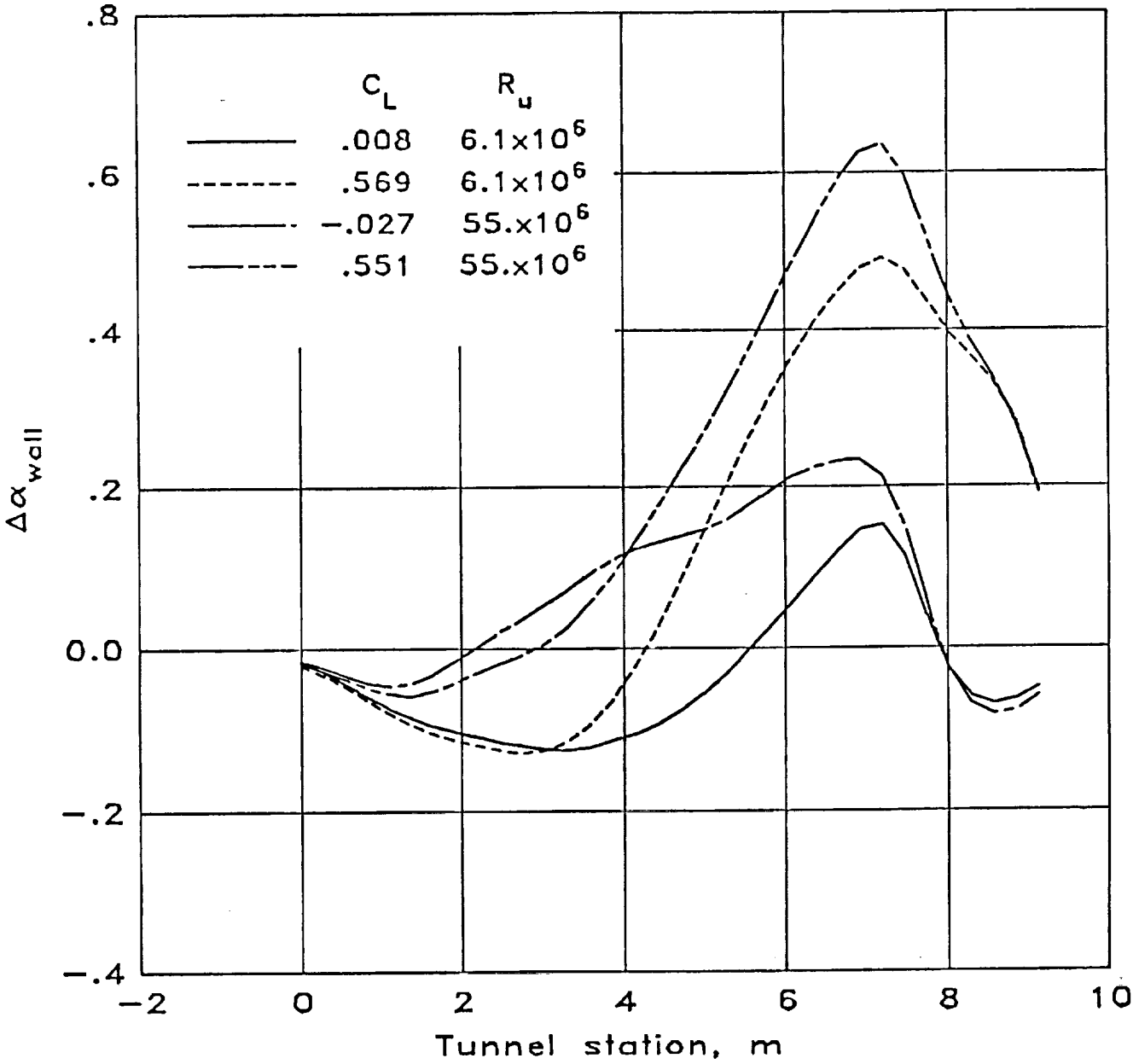

b. Flow angle component of wall interference.

Figure 24. Concluded.

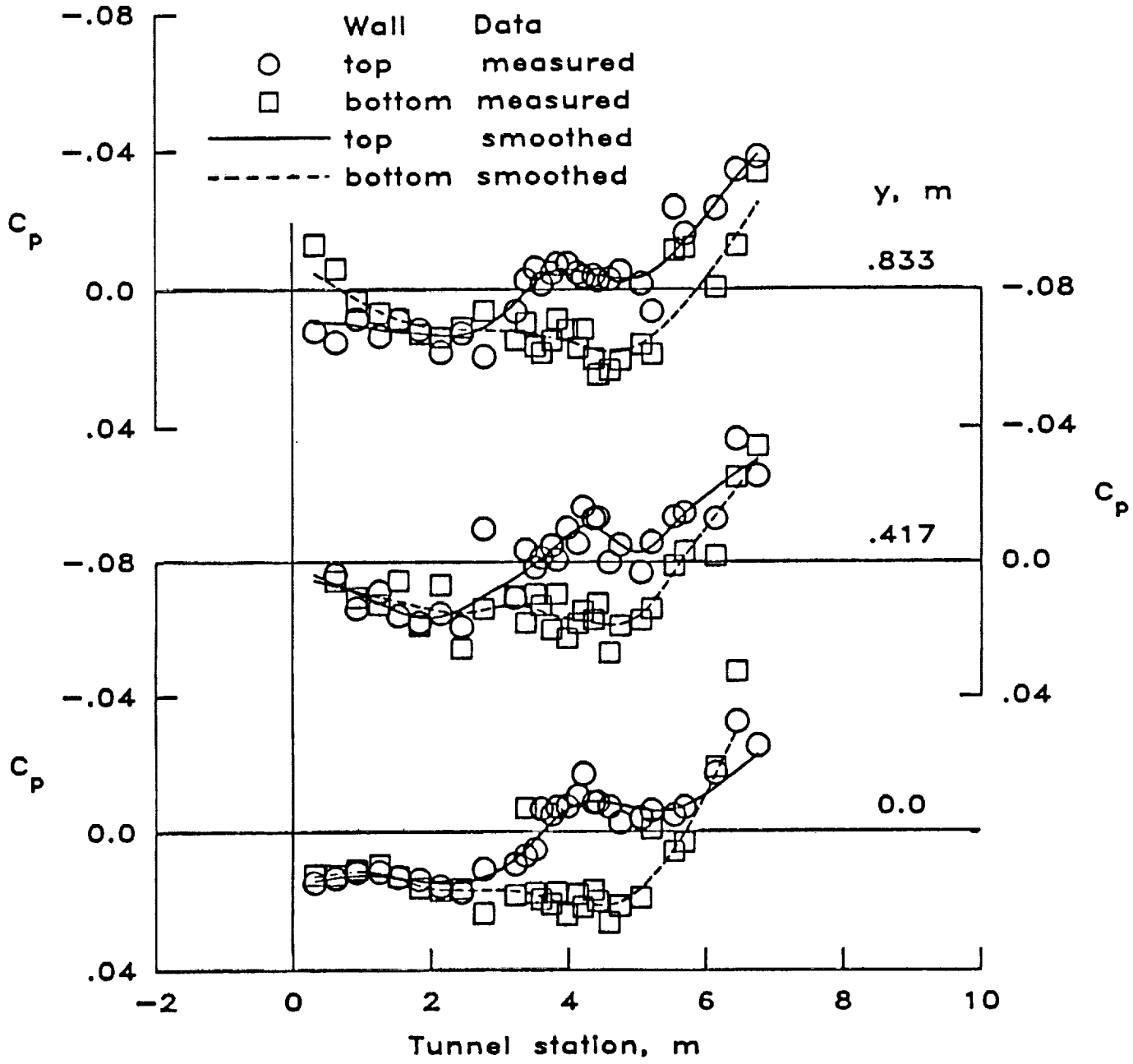

a. $R_u = 6.1 \times 10^6$, $\delta_w = -0.11$ deg., $C_L = 0.569$.

Figure 25. Longitudinal distribution of measured and smoothed pressure coefficients on the three rows used for wall pressure specification on each of the top and bottom walls for two of the test points of figure 24.

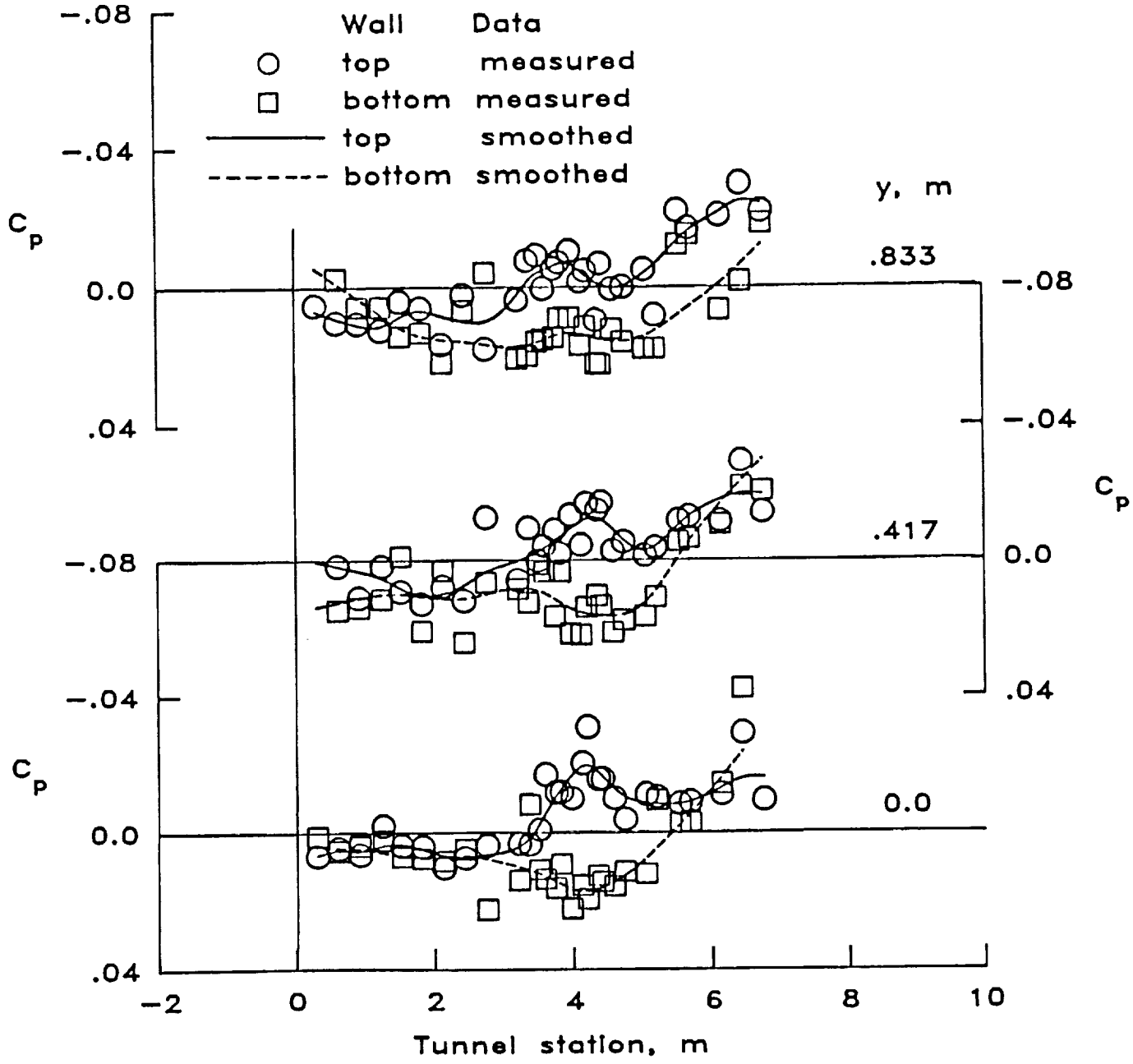

b. $R_u = 55 \times 10^6$, $\delta_w = 0.03$ deg., $C_L = 0.551$.

Figure 25. Concluded.

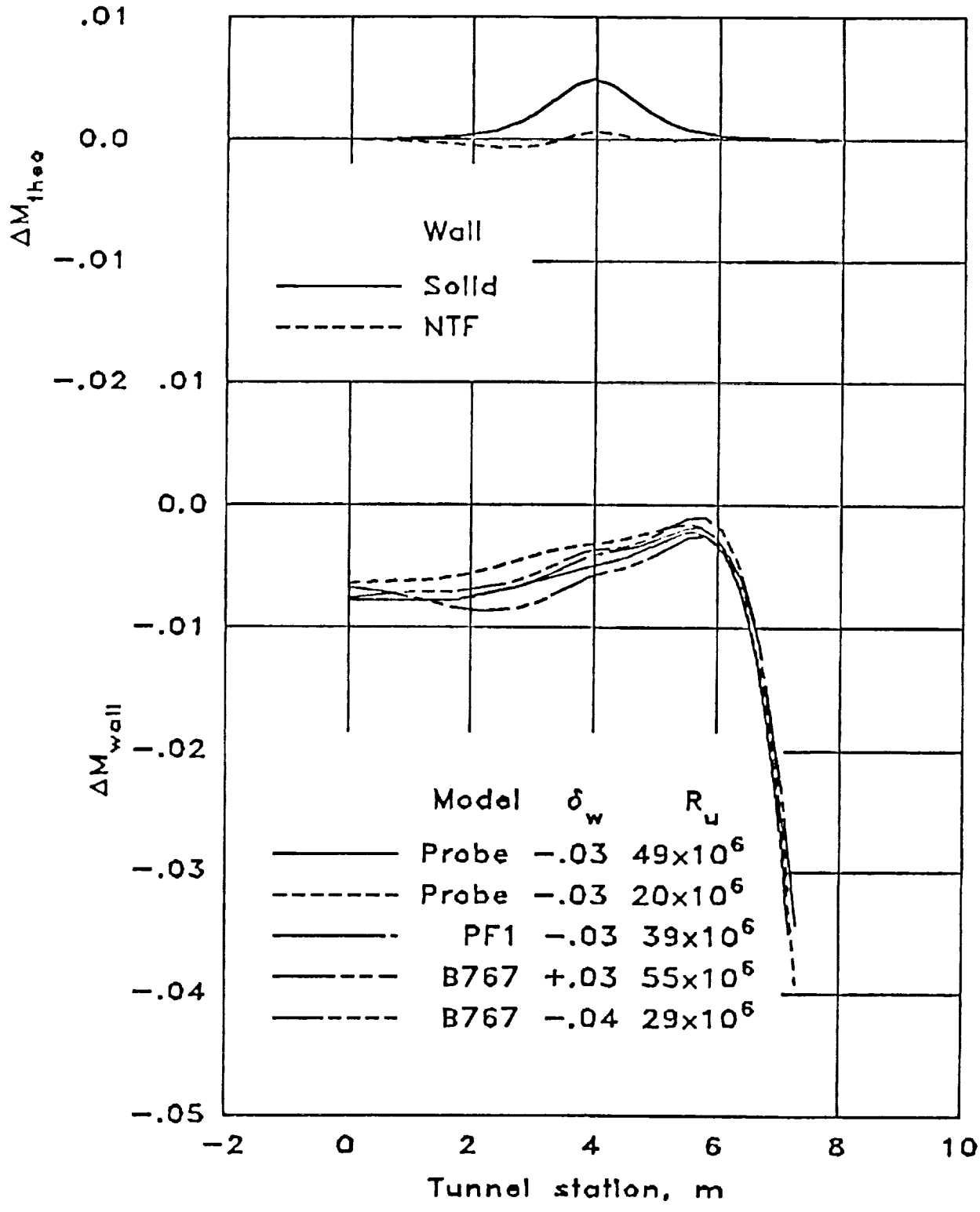

Figure 26. Effect of model installation on Mach number component of assessed wall interference distribution on a survey line at $y = 0.625$ m, $z = 0$. Theoretical distribution on tunnel center line from reference 14 included for comparison.

NASA
National Aeronautics and Space Administration

Report Documentation Page

1. Report No.	2. Government Accession No.	3. Recipient's Catalog No.
NASA CR-4352		

4. Title and Subtitle	5. Report Date
Description and Evaluation of an Interference Assessment Method for a Slotted-Wall Wind Tunnel	April 1991
	6. Performing Organization Code

7. Author(s)	8. Performing Organization Report No.
William B. Kemp, Jr.	
	10. Work Unit No. 505-59-54-01

9. Performing Organization Name and Address	11. Contract or Grant No.
ViGYAN, Inc. 30 Research Drive Hampton, VA 23666-1325	NAS1-18585
	13. Type of Report and Period Covered
12. Sponsoring Agency Name and Address	Contractor Report
National Aeronautics and Space Administration Langley Research Center Hampton, VA 23665-5225	14. Sponsoring Agency Code

15. Supplementary Notes

NASA Langley Technical Monitor: Jerry B. Adcock

16. Abstract

A wind-tunnel interference assessment method applicable to test sections with discrete finite-length wall slots is described. The method is based on high order panel method technology and uses mixed boundary conditions to satisfy both the tunnel geometry and wall pressure distributions measured in the slotted-wall region. Both the test model and its sting support system are represented by distributed singularities. The method yields interference corrections to the model test data as well as surveys through the interference field at arbitrary locations. These results include the equivalent of tunnel Mach calibration, longitudinal pressure gradient, tunnel flow angularity, wall interference, and an inviscid form of sting interference. Alternative results which omit the direct contribution of the sting are also produced. The method has been applied to the National Transonic Facility at NASA Langley Research Center for both tunnel calibration tests and tests of two models of subsonic transport configurations.

17. Key Words (Suggested by Author(s))	18. Distribution Statement
Slotted walls Wall interference Interference assessment Wind-tunnel corrections	Unclassified - Unlimited Subject Category 09

19. Security Classif. (of this report)	20. Security Classif. (of this page)	21. No. of pages	22. Price
Unclassified	Unclassified	51	A04

NASA FORM 1626 OCT 86

NASA-Langley, 1991